Foams pore size estimation and their acoustic properties.

Bc. Tomáš Matoušek

Diplomová práce
2009

Univerzita Tomáše Bati ve Zlíně
Fakulta technologická

Univerzita Tomáše Bati ve Zlíně
Fakulta technologická
Ústav inženýrství polymerů
akademický rok: 2008/2009

ZADÁNÍ DIPLOMOVÉ PRÁCE

(PROJEKTU, UMĚLECKÉHO DÍLA, UMĚLECKÉHO VÝKONU)

Jméno a příjmení:	**Bc. Tomáš MATOUŠEK**
Studijní program:	**N 2808 Chemie a technologie materiálů**
Studijní obor:	**Inženýrství polymerů**
Téma práce:	**Odhad velikosti pórů v pěnách a jejich akustické vlastnosti.**

Zásady pro vypracování:

1. **Literární rešerše problematiky**
2. **Obstarání materiálů s otevřenými póry**
3. **Vyvinutí metody pro získání obrazu rovinného řezu strukturou**
4. **Analýza velikosti pórů pomocí metody EDM**
5. **Návrh a otestování alternativních metod určení velikosti pórů**
6. **Zjištění akustických vlastností materiálů**
7. **Analýza vlivu struktury na akustické vlastnosti**

Rozsah práce:

Rozsah příloh:

Forma zpracování diplomové práce: **tištěná/elektronická**

Seznam odborné literatury:

1. **Pispola G, Horoshenkov KV, Khan A.: Comparison of two modeling approaches for highly heterogeneous porous media. J. Acoust. Soc. Am. 2007 Feb; 121(2):961-6.**
2. **Lu TJ, Chen F, He DP: Sound absorption of cellular metals with semiopen cells J. Acoust. Soc. Am. 2000 108(4), 1697-1709.**
3. **Shen HB, Nutt S, Hull D: Direct observation and measurement of fiber architecture in short fiber-polymer composite foam through micro-CT imaging, Composites Science and Technology 2004, 64(13-14), 2113-2120**
4. **Saxl I, Ponížil P: Grain size estimation: w - s diagram. Materials Characterization 46 (2001), 113 - 118.**

Vedoucí diplomové práce: **doc. RNDr. Petr Ponížil, Ph.D.**
Ústav fyziky a mater. inženýrství

Datum zadání diplomové práce: **11. února 2009**

Termín odevzdání diplomové práce: **15. května 2009**

Ve Zlíně dne 11. února 2009

doc. Ing. Petr Hlaváček, CSc.
děkan

UNIVERZITA TOMÁŠE BATI VE ZLÍNĚ
Fakulta technologická
L.S.

doc. Ing. Roman Čermák, Ph.D.
vedoucí katedry

ABSTRAKT

Diplomová práce se zabývá zjišťováním velikostí pórů v polymerních pěnách s otevřenými póry a vztahem mezi jejich strukturou a akustickými vlastnostmi. Byla navržena metoda vizualizace rovinné plochy měkké polyuretanové pěny. Vizualizace byla provedena u pěti vybraných vzorků s různou pórovitostí. Získané obrazy byly podrobeny obrazové analýze, z níž byla odhadnuta velikost pórů a distribuce jejich velikostí. Následně byly měřeny akustické vlastnosti zkoumaných materiálů a studován vztah mezi strukturou a akustickými vlastnostmi.

Klíčová slova: Polymerní pěna, polyuretan, velikost pórů, akustické vlastnosti.

ABSTRACT

The Master Thesis is focused on estimation of pore size in polymeric foams with opened-pores and relations between structure of pores and acoustic properties. The method for visualization planar section of flexible polyurethane foam has been suggested. Visualization was carried out for five selected samples with different porosities. Obtained images were analyzed by image analysis. Thus the pore sizes and distribution of sizes were estimated. Then the acoustic properties of observed materials were measured. Finally the behaviour between structure and acoustic properties was studied.

Keywords: Polymer foam, polyurethane, pore size, acoustic properties.

Acknowledgments - poděkování

Rád bych využil tohoto místa, abych poděkoval panu Doc. RNDr. Petru Ponížilovi, Ph.D, vedoucímu mé diplomové práce, který ochotně a trpělivě odpovídal na mé dotazy související s problematikou diplomové práce a věnoval mi nemálo svého volného času, čímž výrazně napomohl ke vzniku této práce.

Velké poděkování patří mým rodičům, kteří mě po celou dobu studia podporovali jak hmotně, tak mentálně.

Nesmím zapomenout také na poděkování všem pedagogům, kteří mi po dobu studia předávali své znalosti a spolužákům, se kterými jsme se jako správný kolektiv vzájemně motivovali při studiu.

I declare, I worked on this Master Thesis by myself and I have mentioned all the used literature.

Zlín, 5/15/2009

…….....
Signature

TABLE OF CONTENT

INTRODUCTION

It seems to be that nowadays – at the beginning of the 21st century not many things rest to be investigated or developed in the field of science and technology. The era of great discoverers and epoch-making inventions is over, though still there are some opportunities how to contribute to overall knowledge of mankind.

Many studies points at mutual relationships between structure, physical (and sometimes chemical) properties of observed material. The same case is this thesis. It is focused on the several main sub-topics. The problematic of stereology of porous material – the polyurethane foam concretely is the first of it. Next subject, which relate to the first one, is the estimation of pores size and distribution of sizes. Third sub-topic is attended to measurement of acoustic properties of selected material and observation of relationships between structural and acoustic properties of polyurethane foam.

These topics are not new. Main goals of this thesis are to summarize present state of art, to offer another point of view to this problematic and compare with the original opinions and, maybe, to help people interested in this branch.

I. THEORETICAL PART

1 DEFINITION OF TERMS

The topic of this thesis – investigation of polymer foams and its acoustic behaviour brings a few main key words. The meaning of these terms will be defined in this chapter.

1.1 Dispersion

Dispersion is a system of at least two kinds of matter (liquid, solid or gas), whereas one kind is dispersed into the second one in the form of small particles. Continuous dominant phase, usually called matrix, surrounds non-continuous dispersed particles.

Dispersions can be divided according to several criteria (e.g. differences of size dispersed particles) into a few sub-groups [1]. One of the most used dividing, shown in table (Tab. 1) is according to state of matter of dispersion's components.

Tab. 1: Classification of dispersions according to state of matter of dispersion's components [1].

dispersed particles	**matrix**		
	solid	*liquid*	*gas*
solid	solid sol	suspension	aerosol (smoke)
liquid	liquid dispersion in surroundings of solid matter	emulsion	aerosol (smoke)
gas	solid foam	foam	/

1.2 Foam

In accordance with table (Tab. 1) the foam can be defined as a heterogeneous system (dispersion) that includes gas particles (mostly air bubbles) in liquid matrix. Similarly we can define the solid foam as a system of air bubbles surrounded by solid matrix Into the group of solid foams belong all cellular materials including polymer foams, which are the subject of interest in this work.

1.3 Acoustics and acoustic properties of material

1.3.1 Acoustics

Acoustics is a large-scale branch. Acoustics studies sound, which is token of oscillation of mass with any frequency between 20 and 20 000 oscillation per second, and noise (any undesirable sound) – from their origin, propagation in the space to its perception

by the people. Acoustics has many sub-branches such as musical acoustics, architectural acoustics, physiological acoustics and others [2].

1.3.2 Waves

The wave is (in conjunction with particle) basic term in classical physics. It is a way of transfer of energy in real time. The basic splitting of waves includes three types:

- Mechanical waves (e.g. water waves or waves of noise),
- electromagnetic waves (e.g. visible light or RTG waves),
- de Broglie's waves (flow of elementary particles).

Mechanical waves, which are the cause of noise, can be subdivided to longitudinal and transversal waves. Sound rises thanks to oscillating of mass (generally every system of points). Oscillation is physical process in which the characteristic values (location, velocity etc.) are changed periodically, in dependence on time.

Noise can propagate as longitudinal waves in every case, in addition as transversal waves in solid mass. In free space noise propagates to all directions [2] and [3].

1.3.3 Basic acoustic quantities

The wavelength λ [m] is the first from fundamental acoustic quantities described in this chapter. It describes a distance between two neighbouring maxima of wave. It can be also defined as a distance, which the wave travels during the time of one oscillation (one period T [s]).

The frequency f [Hz] is physical quantity showing number of cycles any periodical phenomenon per time unit. Relation between wavelength, frequency and period is shown in equation (1) [4]:

$$\lambda = \frac{c}{f} = \mathrm{c}T\,, \tag{1}$$

where c is velocity of wave.

Passing of acoustic wave through some surrounding space causes to the pressure fluctuations. Overall pressure in this place balances around original pressure. This variable pressure is called acoustic pressure p [Pa]. It is defined by the equation (2) [4]:

$$p = \frac{p_0}{\sqrt{2}}, \tag{2}$$

where p_0 is amplitude of wave.

Acoustic wave transfers mechanical energy from source (oscillating system) to surrounding space. Quantity of this energy, which passes imaginary unit area per time unit, is acoustic power P [W]. This quantity is a basic parameter of all sources of noise. Equation (3) is definition of this quantity [4]:

$$P = \frac{Fs}{t} = Fc = pcA, \tag{3}$$

where F is force, s is trajectory, A is area, c is velocity and t represents time.

Soundproofing properties of materials are commonly called transmission loss characteristics. Transmission loss ξ [-] denotes ability of material to resist propagation of acoustic energy through material. As it is shown by the equation (4) the transmission loss is defined as a ratio between acoustic powers after transmission of noise through material P_2 and primary value of acoustic power P_1. This quantity strongly depends on the incidence angle Φ of noise and angular frequency ω ($\omega = 2\pi f$) of waves [4].

$$\xi(\Phi, \omega) = \frac{P_2(\Phi, \omega)}{P_1(\Phi, \omega)} \tag{4}$$

When the acoustic waves run into the surface of some mass there is an interaction between waves and mass. Part of acoustic energy is reflected, next part passes through and rest of it is absorbed. Different materials has different ratio between these three parts of energy. The absorbed part is transferred to another kind of energy, mainly to the thermal energy. Acoustic absorption is defined as a ratio of absorbed acoustic power divided by total acoustic power of noise. The ratio illustrated in equation (5) is commonly called absorption coefficient α [-] [4]:

$$\alpha = \frac{P_A}{P} = 1 - \left|R^2\right|, \tag{5}$$

where, P is total acoustic power, P_A is acoustic power absorbed by the material and R [-] is reflection coefficient.

The value of α can be inside the interval <0; 1> whereas value α = 0 describes a material without absorption of noise and α = 1 means total absorption of noise. Surface

absorption of noise is a function of many parameters such as roughness, porosity and acoustic compliance [4].

Specific acoustic impedance; Z [N.s.m^{-3}]

Specific acoustic impedance or wave resistance of material is defined by following equation (6) [5]:

$$Z = \rho.c = \frac{p}{v}, \tag{6}$$

where ρ is density of material and v is speed of oscillating of particles.

The last discussed acoustic quantity is acoustic intensity **I** [W.m^{-2}]. Size of this vector quantity shown in equation (7) describes quantity and direction of acoustic energy flow. Upright to the direction of acoustic wave acoustic intensity equals zero [4].

$$I = \overline{p(t).v(t)} \tag{7}$$

1.3.4 Other important terms

Human ear cannot respond to any acoustical stimulus linearly – the perception of it is proportional to the logarithm of this stimulus. That is the reason for implementation of term acoustical level. Acoustical level is defined as a common logarithm of ratio between observed quantity and any reference value:

$$L = \log\frac{X}{X_0} = \log\frac{\text{compared value}}{\text{reference value}} \tag{8}$$

The basic unit of acoustical level is bel [B] (named after inventor of phone A. G. Bell). Because of better interpretation the dB – decibel (= 0,1 B) is commonly used [4].

2 POLYMER FOAMS

The polymer foam has been chosen for estimation of pore size as it was discussed in chapter 1.2. This dispersion system consist any polymeric matrix, which surrounds a "bubbles" of air. These cavities are frequently called cells or pores. The polymer/air ratio (which determines a density of material) also as the pore size may vary – depending on manufacturing conditions [6].

There are two important macroscopic characteristics of polymer foams highly affected by the structure in term of applications. Mechanical properties are first of it. Mechanical properties of polymer foams are influenced by two parameters: density and morphology of cells [7]. The same importance has acoustical properties. This important macroscopic value plays an important role in applications of polymer foams. Acoustical properties depend on pore size [8] and [9].

2.1 Foamed polymers

Wide group of polymers is used for technical applications as foam. Both closed- and opened-foams are often used in automotive, building industry, packaging industry and others industrial branches. Commonly exploited polymer foams are PE, PP, PS, PVC, EVA and PPO-PS blend. All of these foams has closed cells. Typical foam with opened cells is PUR foam [10].

2.2 Classification of polymer foams

The main classification of polymer foams is usually carried out from structural point of view. As it is shown in figure (Fig. 1), there are two basic types of polymeric foams – – foams with opened cells (Fig. 1a) and closed-cell foams (Fig. 1b). The picture shows also its structural differences – faces of pores. Open-cell foams have the most of faces open whereas in case of closed-cell materials there is the opposite situation [10].

There are few opposing views concerning shape of pores. It can differ depending on production conditions. Extruded foams with closed-cells have ellipsoidal shape of cells because of melt deformation in flow direction during processing [7]. Another shapes of cells (rectangular, triangular, hexagonal or polyhedra with 10-17 faces) are also available [6], [10]. Therefore there are some opinions assuming spherical shape of pores [11], [12].

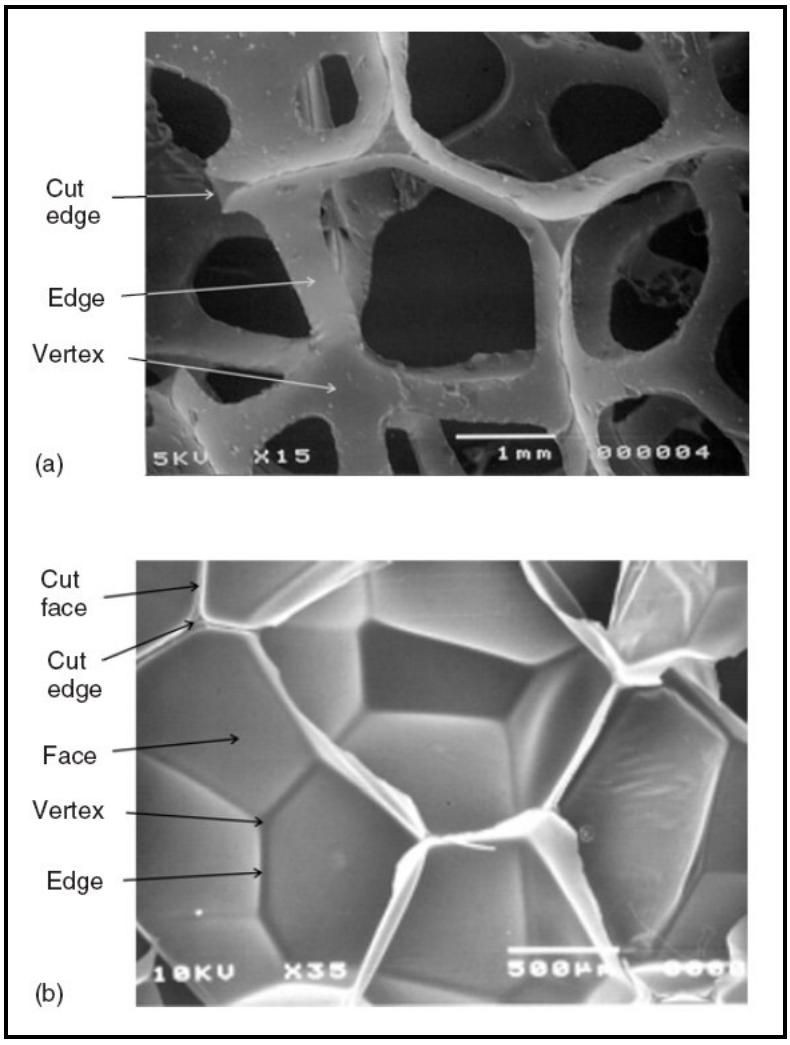

Fig. 1: SEM pictures of open-cell and closed-cell foams [10].

2.3 Observed material – flexible polyurethane foam

The polymers known as polyurethanes (PUR) include materials that incorporate the carbamate group, -NHCOO-, as well as other functional groups, such as ester, ether, amide, and urea. The name polyurethane is derived from ethyl carbamate, known as urethane.

2.3.1 Production

These polymers are usually produced by the polyaddition reaction of polyfunctional isocyanate with a macroglycol, a so-called polyol, or other reactants containing two or more groups reactive with isocyanates. This addition polymerization reaction, to produce urethane polymers was pioneered in 1937 by O. Bayer [13]. The chemical reaction is generalized by (9):

$$R\text{-}N{=}C{=}O + H\text{-}0\text{-}R` \rightarrow R\text{-}NH.COO\text{-}R`, \quad (9)$$

where R and R’ are radicals (e.g. phenyl group) [14].

Monomers – isocyanates and polyols can vary in dependency on foam type. Flexible PUR foams (with open cells) are often based on toluene-2,4-diisocyanate shown in figure (Fig. 2a), whereas rigid PUR foams (closed cell types) are usually made from 4,4'-methylene diphenyl diisocyanate (Fig. 2b). As a polyol the glycols, polyglycols and hydroxy-polyesters are widely used [14].

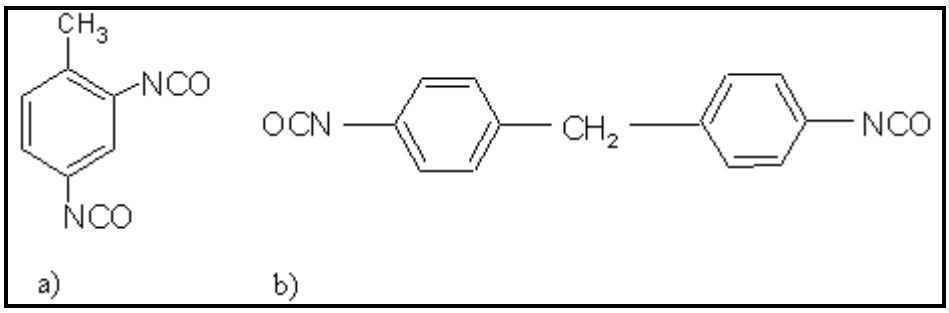

Fig. 2: a) toluene-2,4-diisocyanate, b) 4,4'-methylene diphenyl diisocyanate [14].

2.3.2 Basic properties, advantages and applications

The reason of investigation this material is obvious: this kind of material is widespread in many applications. A major advantage of this material is that it can be manufactured with relative ease to varying densities, which are only a few percent of the density of the base material. It has excellent energy absorption characteristics and it is widely used for shock mitigation in automotive, in packaging and in cushioning. Polyurethane foams are also widely used as cores in sandwich plates and shells, which is one of the most effective weight saving design options for structures in a variety of applications. The advent of carbon and ceramic has recently enabled the use of such construction in high temperature applications in jet engine nacelles and rocket nozzles [6]. In present also the polyurethane composite systems become popular [15], [16] and [17]. Practical usage of polyurethane foam with opened cells as a damping material for noise and vibrations is also possible [18].

STEREOLOGY OF POLYMER FOAMS

2.4 Stereology

Stereology is the study of three-dimensional structure, and particularly the measurement of key parameters describing that structure based on two-dimensional images. In most cases these images are obtained by microscopy (optical, electron, etc.) but another methods providing two-dimensional images can be chosen.

Two basic stereological approaches are often used. First of it suppose that structure of material is deterministic just only probes (selections) are random. Second approach is based on modeling of structure by random processes [19].

For valid application of stereology it is necessary to know relationships between two-dimensional image and three-dimensional object. For a planar section through a structure, volumes appear as areas, surfaces appear as lines, and lines appear as points. Measurement of these areas, lines, and points does not directly determine the extent of the three-dimensional structure, but can be used to calculate an estimator [20]. There are three ways how to obtain pore volumes [21], as it will be discussed later.

2.5 Observation of porous or grainy materials

Studying of real structure and subsequent quantitative stereological evaluation of obtained images is the simplest way of stereological description of material. There are several methods for observation of porous or grainy samples. Some of frequently used will be described in this chapter.

2.5.1 Microscopy

Microscopy is technique of observation small objects or small details on bigger objects. There are many kinds of microcopies – the most frequently used are optical microscopy (OM), scanning electron microscopy (SEM), transmission electron microscopy (TEM) and atomic force microscopy (AFM). Tanks to their reliability, microscopical methods are widespread for examination of architecture of cells (or grains) in biology, metallurgy, and polymer science [22], [23] and [24]. In term of polymer foams it can be used for observation both closed-cell [7] and opened-cell foams [16].

The principle of microscope is an interaction of sample with photons (OM) or electrons (SEM, TEM) emitted from source towards to sample or measurement of atomic forces between tip of microscope and sample (AFM). OM and SEM are based on detection of reflected photons (OM) and electrons (SEM) whereas TEM detects electrons transmitted throughout the ultra thin sample. AFM examines changes of quantity intermolecular interactions between the tip and sample, which describes topology of sample's surface.

Resolution ability of microscopy depends on wavelength of used radiation and increases from optical microscope through SEM and TEM to AFM. Each of these methods is specific and provides different images but all of these methods can represent the image of structure satisfactory [25].

2.5.2 Computer tomography

Computer tomography (CT) is nondestructive digital imaging technique. The word "tomography" is derived from the Greek words τομή (slice) and γράφω (to write). CT is based on the recording the attenuation of radiation (x-ray) after passing through investigated object from several directions. The computer from cross sections of projections reconstructs resulting image. This method was initially implemented in the medical field; nowadays it is also used in materials research [26].

In context of the topic, CT images are often used as planar section images for following image analysis and estimation of pore section size [21] or volume of pores [27]. CT can be also applied on observation of distribution of filler in foamed composite systems [28].

2.5.3 Another methods

Another methods used for characterization of grainy or porous systems are mercury porosimetry and laser diffraction.

Mercury porosimetry (or mercury intrusion porosimetry) is an important and widely used technique for the analysis of the pore structure of a variety of porous materials. It is based on the gradual intrusion of mercury into an evacuated porous system as an external pressure is applied; increasing pressure makes smaller pores accessible to mercury. This method allows obtaining pore size distribution [29].

Laser diffraction technique is based on the diffraction of laser beam by the sample. When the particle size is significantly larger than the incident wavelength with a refractive index significantly different from the surrounding medium, most of the light is scattered in the forward direction at small angles relative to the propagation direction of the incident beam. This technique is popular in the field of powder systems [30].

2.6 Modeling of structure

Modeling of structure is second stereological approach. Using a model structure, physical properties of the corresponding material are simulated. Repeated calculations with varying model parameters allow investigating how the material's properties change with altering microstructure. Thus, instead of producing many sample structures and choosing the best one for a given application, suggestions for good candidates can be obtained by simulation. The increasing capability of simulation algorithms as well as computer power allows for high precision in the simulation results. In return, this requires more and more sophisticated model structures and model fitting procedures [31].

Thanks to presented advantages, modeling of structure is very popular tool in materials research. By using different models and approaches, varying properties of material are predicted.

2.6.1 Tessellation

Tessellation is term, describing a method of partition of space to final number of cells, which fills this space particularly or totally and which has at most one border in common. In case of total filling the space is called tessellation. Particularly filled space is an example of incomplete tessellation. The simplest partition consists in comparing distances of points in space from the center of cells. Those points fill inner space of cell, which are closer to the one cell center then to another ones. The cells borders are created by the points, which have the same distance to more than one cell center.

Dislocation of centers in space is called point process. Centers can be distributed homogeneous – mutually independent – in empty Euclidean space – it responds to Poisson point process, or inhomogeneous. Inhomogeneous distribution may be caused of mutual interactions between centers (attractive or repulsive interactions). An attractive interaction leads to clustering of centers and forms cluster fields. In the second case distances between

neighbouring centers may be bonded below by repulsive interactions, which forms models with hard core.

Periodical distribution of centers is the simplest: centers makes translation grid and all cells has the same size and in addition it has the same orientation. This case of periodical distribution is unreal in real objects, but sometimes there is tendency to go near to this situation as much as possible – as an example the tendency of periodical distribution of filler in composites can be used. These "grid systems" are described by Bookstein's model and tessellation generated by this model. Thanks to tessellations the grainy, porous or polycrystalline material can be model [11], [32] and [33].

2.6.2 Voronoi tessellation

Voronoi tessellation is one type of tessellation. This tessellation can be assigned to all system of points and it has the unique solution for most of it. Very important property of Voronoi tessellation is convexity of cells. There are several definitions of Voronoi tessellation. The Growth model, shown in figure (Fig. 3) is one of it.

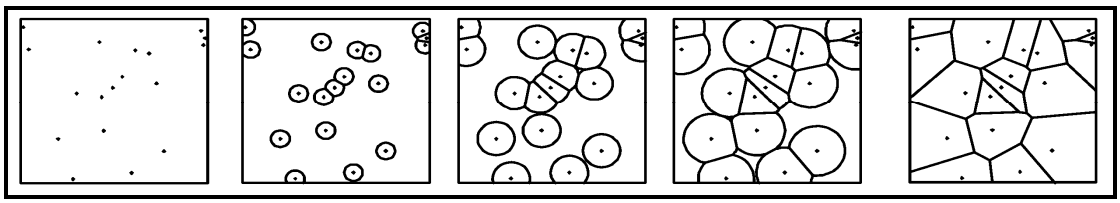

Fig. 3: Growth model of spherutical growth in polymer melt; t = 0 on the left; t = ∞ on the right [33].

This model expects start of growth objects (grains, cells, etc.) from nuclei in time $t = 0$. The velocity of growth from all nuclei is constant. Growth of objects is terminated in every point of contact with neighbouring object. The objects created by this way represent the Voronoi tessellation. Growth model can be used for modeling of progression material microstructure [33]. Except this, Voronoi tessellation can be used in many other fields such as astronomy, biology physics and logistics [32].

2.6.3 Poisson-Voronoi tessellation

Poisson-Voronoi tessellation (PVT) is Voronoi tessellation generated by Poisson point process. Generated points are distributed homogenously in space. The cells of PVT (shown in figure (Fig. 4) correspond to this distribution [32].

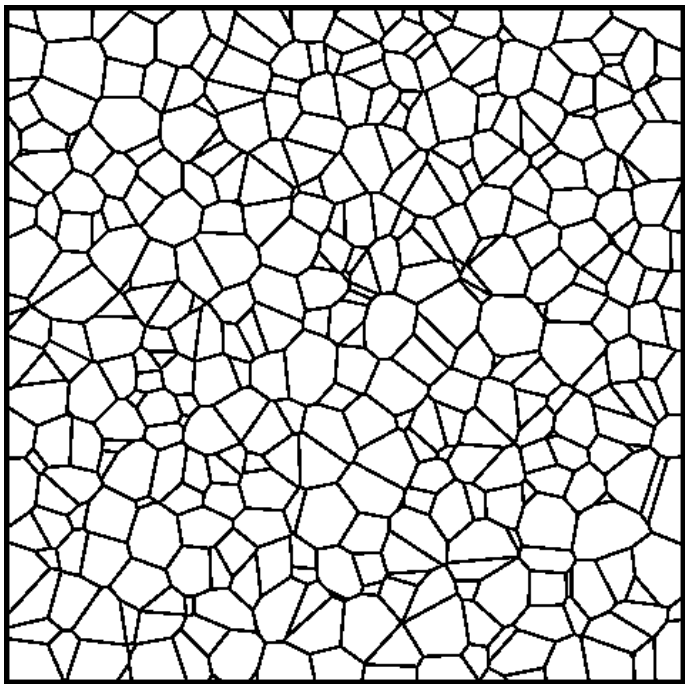

Fig. 4: Planar section of three-dimensional Poisson-Voronoi tessellation [12].

2.7 Modeling of fluid flow

2.7.1 Biot viscosity correction function

Biot viscosity correction function, represented by equations (10), (11) and (12) used e.g. by Pispola et al. [9] is a mathematical description of arbitrary pore size distribution approach. It is the ratio of the average viscous friction force on the capillary walls per unit bulk volume to the average seepage velocity per unit bulk cross-sectional area and measures the deviation from the Poiseuille flow friction (the friction between air molecules inside the pores is dominant). For a porous material with circular cylindrical pores with radius r with probability density function (PDF) $f(r)$, the viscosity correction function F_{BVC} is given by the following expression:

$$F_{\mathrm{BVC}}(\omega) = \frac{1}{4} \frac{\int_0^{\infty} \kappa T_{\mathrm{B}}(\kappa) f(r) \mathrm{d}r}{\int_0^{\infty} \left[1 - 2\kappa^{-1} T_{\mathrm{B}}(\kappa)\right] f(r) \mathrm{d}r}, \tag{10}$$

where parameters T_B and κ are defined as:

$$T_B(\kappa) = \frac{I_1(\kappa)}{I_0(\kappa)}, \tag{11}$$

$$\kappa = r\sqrt{\frac{\omega\rho_0}{\eta}}, \tag{12}$$

where I_1 and I_0 are the modified Bessel functions, ρ_0 [kg.m^{-3}] is the equilibrium density of air, η [Pa.s] the dynamic viscosity of air and ω [rad.s^{-1}] the angular frequency. Solution of the viscosity correction function (9) via direct numerical integration requires data on PDF $f(r)$ [9].

2.7.2 Double porosity approach

Flow and transport in structured porous media are frequently described using double porosity (or dual-porosity) models. This problematic was firstly defined in geology [34] but the general double porosity theory is applicable also for polymer foams [9] and [35].

In double porosity models the void space of the fractures (pores) is considered as a continuum while the void space within the blocks (polymer) is regarded as another continuum. The dual-porosity medium is considered to be a superposition of these two systems over the same volume. The two pore systems interact by exchanging air, water, or solutions in response to pressure head and concentration gradients. Macroscopically, two flow velocities, two pressure heads, and two solute concentrations characterize the porous medium at any point in time and space. Dual-porosity (DP) models assumes that both fluid flow and solute transport can be described by two equations, which are coupled through a term that describes the exchange of fluid or solute between the two pore regions [36].

The DP can be employed to model the acoustic behaviour of materials with two distinct pore scales: meso-porous scale l_p (represents a group of pores with size 1,12-4,14 mm) and micro-porous scale l_m (pore size between 0,04-1,64 mm). The model is based on assumptions of low ratio (l_p/l_m) between the characteristic dimensions of the meso- and micro-porous parts of the medium and ability of macroscopic nonacoustic quantities (total flow resistivity ψ_{db}, total open porosity Ω_{db}, flow resistivity of micro-scale ψ_m, open porosity of micro-scale Ω_m, flow resistivity of meso-scale ψ_p and open porosity of

meso-scale Ω_p) to characterize the micro- and meso-porous parts [9]. These quantities are described by following equations (13) and (14):

$$\Omega_{db} = \Omega_p + \Omega_m(1-\Omega_p) = \frac{A_{fp}}{A} + \left(1-\frac{A_{fp}}{A}\right)\frac{A_{fm}}{A-A_{fp}}, \tag{13}$$

where A_{fm} is area occupied by micro-scale, A_{fp} is area of meso-pores and A is the total area of sample surface.

$$\frac{1}{\Psi_{db}} = \left[\frac{(1-\Omega_p)}{\Psi_m} + \frac{1}{\Psi_p}\right] \tag{14}$$

2.8 Image analysis

Image analysis is a process that serves for evaluation of digital images from stereological point of view. The goal is to get reproducible and representative data describing the observed structures typically. This process is includes:

- Image recording and its transformation to the digital form,
- image corrections,
- identification of objects (grains, cells, etc.),
- quantification to finite number of data.

Recording of source data – images of planar sections of samples is described in previous chapter (2.5). Transformation of image to the digital form is carried out thanks to the CCD cameras (OM) or created directly by the software pertaining to the device (SEM, TEM, AFM).

Image corrections includes selection of square or rectangular area from the whole picture, noise removing, contrast adjustment and colour transformation. Noise arises during the transformation of image from analogue form to the digital one and affects the results of measurement. Colour transformation and contrast adjustment as well are necessary to. Images are transformed from the coloured original to the black and white form. These are required for objects identification.

Identification of objects is the most important part of image analysis. Transformed black and white image is divided to the objects (cells, grains, etc.) and their background.

Founded objects are described by finite number of data (corresponding with number of objects) representing the characteristic values of investigated objects such as diameter or area. For correct interpretation many measurement have to be done and the statistical methods of evaluation must be used [37].

2.8.1 Euclidean distance map

Euclidean distance map (EDM) is a basic tool often used in image analysis [21], [27], [38] and [39]. EDM coming out of pattern (black and white image), which is divided to the two sets of points in p rows and q columns (according to the resolution – one pixel = one point). The first set represents a group of object (foreground) with associated value $b_{pq} = 1$ and the second group describes empty space (background) with value $b_{pq} = 0$. Subsequently, there is assigned a distance to the closest foreground point to each background point b_{ij}. This distance is computed from equation (15):

$$d_{ij} = \min_{1 \le p,q \le N} \left(\sqrt{(p-i)^2 + (q-j)^2} \,\middle|\, b_{pq} = 1 \right) \tag{15}$$

2.9 Conversion of pore section areas to pore volumes

Information about cell areas are not representative as material characteristic. The conversion of areas to volumes is necessary. In principle, there are three ways how to obtain pore volumes. All of these suppose semi-spherical shape of cells [21].

2.9.1 ASTM E 112

ASTM E 112 is the American standard used for determining average size of grain size in metals [40]. It is based on following equations (16) and (17), describing a relation between mean area $\mathbf{E}A$ of random planar section of sphere and its mean volume $\mathbf{E}V$ ($\mathbf{E}*$ denotes mean value of *):

$$\mathbf{E}V = C`.(\mathbf{E}A)^{3/2} \tag{16}$$

where

$$C` = \sqrt{\frac{6}{\pi}} = 1{,}382 \tag{17}$$

By using these equations it is possible to calculate mean volume of spherical and irregular shapes too. Disadvantage of this method is impossibility to give information about pore size distribution [21].

2.9.2 Geometrical solution

This approach is based on imagination of spherical shape of pores. A sphere of diameter D is the geometrical model of pore. The sphere diameter distribution will be characterized by PDF f_D and the mean $\mathbf{E}D$. Planar section of sphere is a circle profile of diameter d. The profile diameter distribution will be characterized by the PDF f_d, the mean $\mathbf{E}d$. This stereological estimation method is coming out of the Wicksell equation (18) [21]:

$$f_d(d) = \frac{d}{\mathbf{E}d} \int_d^{D_m} \frac{f_D(D)}{\sqrt{D^2 - d^2}} \mathrm{d}D, \tag{18}$$

for $0 \leq \mathrm{d} \leq D_m$, where D_m is the maximum of D and d.

For estimation of an unknown PDF f_D, a model PDF f_D, which depends on some parameters is chosen. Then the model profile PDF f_d can be fitted to the empirical one [27].

2.9.3 Spatial solution

This, the most precise but the most difficult approach, is carried out by the computation of spatial EDM and subsequent spatial Voronoi tessellation. By this solution the size of each pore is known. The problem of this method is enormous computational demandingness of spatial EDM [21].

3 NOISE PROPAGATION AND ABSORPTION

Acoustic properties of any material can be conceived as a summary of properties affecting propagation of noise through given material. Studying of acoustic properties is very important for subsequent applications of studied materials. Ability of noise to propagate through any material depends on mechanism of propagation (or inhibition) inside the medium and relationships effects noise propagation All media have three properties which affect the behavior of noise propagation:

- A relationship between density and pressure. This relationship, affected by temperature, determines the speed of noise within the medium.
- The motion of the medium itself, e.g. wind. Independent of the motion of noise through the medium, if the medium is moving the noise is further transported.
- The viscosity of the medium. This determines the rate at which noise is attenuated. For many media, such as air or water, attenuation due to viscosity is negligible [41].

Term noise absorption generally means conversion of absorbed part of acoustic energy to another kind of energy, usually thermal energy. Rest of acoustic energy is splitted to reflected and passed part [42]. Scheme of interaction between wall and acoustic waves is shown in figure (Fig. 5):

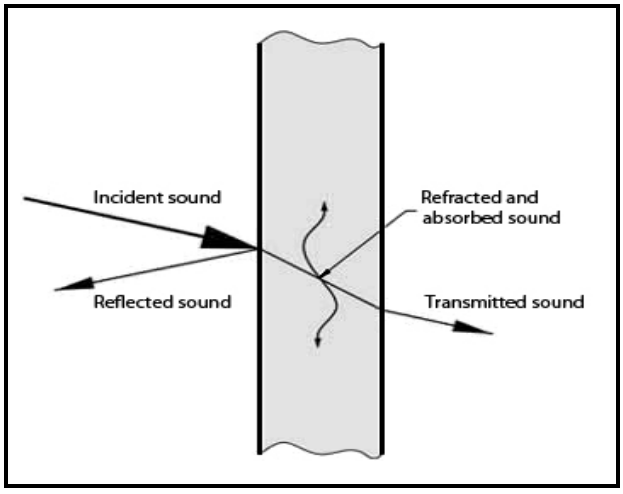

Fig. 5: Reflection, absorbtion and transmission of sound [43].

3.1.1 Absorption of noise in air

This phenomenon is the most common manner of noise absorption in our surroundings. In comparison with other media, propagation of noise in air is very easy. Except of air molecules, there is no significant impediment for acoustic waves. Noise absorption in air varies in dependency on frequency of noise, relative humidity of air and temperature of air. Lower frequencies and higher relative humidities and temperatures cause increased noise absorption [4].

3.1.2 Absorption of noise in porous media

Description of noise absorption is more difficult than in previous case. Decreasing of acoustic energy can be caused by three ways, whereas mostly is the shortage due to the combination of all of them [44]:

- Friction of oscillating air particles with walls of pores:

  While the noise penetrates into the pores of noise absorbing material, the kinetic energy of acoustic field decreases. The effectiveness of this phenomenon rises with increasing porosity of given material.

- Reduction of potential energy of penetrating wave:

  This leads to relaxation of acoustic pressure, which may be caused by heat transfer between air and material. Transition of heat reduces the air temperature and pressure in thinking place.

- Non-reversible deformation of fibers of material (influence of elastic hysteresis):

  Elastic hysteresis is typical phenomenon for polymer foams. It can be caused by every force, which deforms the foam. After termination of action of the force the material has the tendency to come back to the original shape. It means that value of deformation work is bigger than work gained by elastic deformation during the shape recovery. This difference is proportional to the shortage of acoustic energy.

Expect these phenomenon, pores also affect absorption ability of porous media – – especially the number of pores. Shape of pores is also important [42].

II. PRACTICAL PART

4 EXPERIMENT

The practical part of this thesis was focused on development of method, which provides the ability of observing planar cut or surface of polymer foams without using a CT method and measurement of acoustical properties of selected foams. Five samples have been investigated. The densities of them are summarized in table (Tab. 2):

Tab. 2: Density of samples.

Sample	Density [kg.m^{-3}]
A	21,12
D	22,60
E	34,17
F	22,74
G	23,70

Note: Samples B and C were also measured by P&S, but because of small amount of material the samples were discarded.

4.1 Pore size estimation

4.1.1 Visualisation of pores

CT technique (described in chapter 2.5.2) is very comfortable method for visualization of pores in planar section of any porous media. This method gives us images of planar section of sample as black and white pictures, where the black area represents a boundary of pores and white space determines an area of pore sections. Output from the CT measurement is shown in the figure (Fig. 6a).

The main disadvantage of CT method is high cost of apparatus. The demand for development an alternative method to CT covers the demand for "cheaper" method with comparable results.

One possibility is a technique of printing and scanning (P&S). The samples of flexible PUR foams were prepared from the sheets by cutting to the small pieces. Printing area of each sample was approx. 1,5 x 1,5 cm. This area – always the straight edge made during the manufacturing of PUR sheet – was covered with stamping ink and printed to the sheet of paper. Printed image was firstly scanned to transfer it into the digital form (example is shown in the figure (Fig. 6b)), and then adapted in picture-editing SW. All samples were

scanned on resolution 1300 dpi (1 px = 0,0195 mm). It was the necessary to adjust the contrast and crop it. Finally the EDM analysis was succeeded.

All samples was measured thirty times according to following rules:

- Five different pieces from every sample were cut,
- each piece was printed to the sheet of paper six times and scanned,
- 600 x 600 px area from every printed image was selected for image analysis (each one from different place),
- image analysis of every picture was executed to obtain estimation of pore section sizes,

computed data were statistically evaluated.

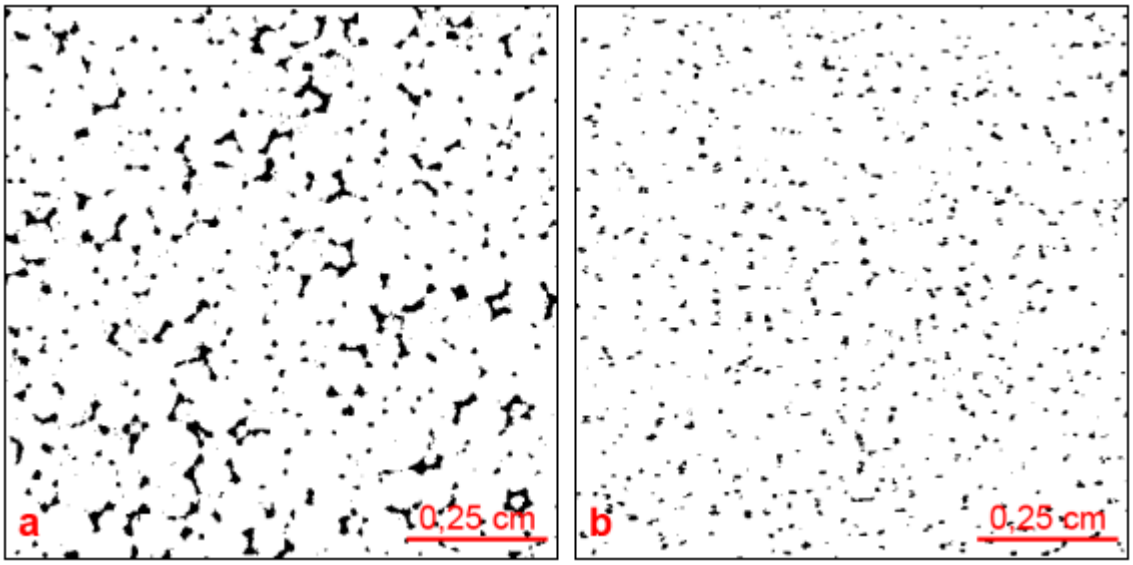

Fig. 6: Comparison of two visualization methods of planar section of flexible PUR sample – CT (1a) [27] and printing and scanning technique (1b).

4.1.2 Image analysis

The image analysis has been carried out by EDM in the SW Tessellation whose environment is pictured in Appendix A I and basic commands are shown in Appendix A II. The image analysis included a several steps. Reduction of noise shown in figure (Fig. 7) was the first one.

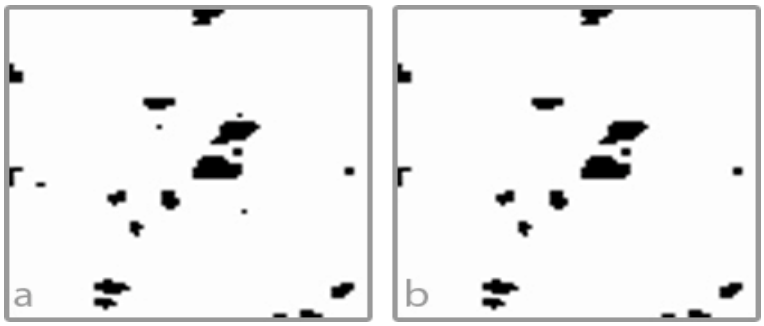

Fig. 7: Detail of P&S image (sample F). Part of original image (4a) and the same part after noise reduction (4b).

The original images were polluted by aggregates of 1-3 black pixels as it is shown in the figure (Fig. 7a). This noise probably originated from both imperfections of paper and noise from scanner. It was necessary to remove it for next measurement. After this operation, only the prints of pore borders were visible as it can be seen in figure (Fig. 7b).

In the second step EDM, based on equation (10) was carried out. Graphical representation of results from EDM computation is shown in figure (Fig. 8). It is not necessary to find distance to each background pixel from each foreground one – only distances from boundary foreground pixels are important (in the figure (Fig. 8) are red). The brightness of the background pixel increases with increasing value of distance:

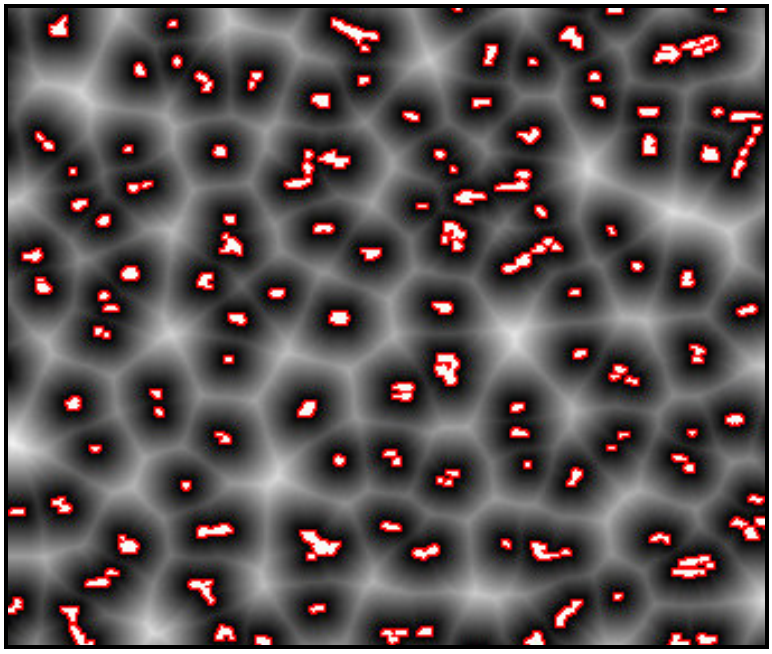

Fig. 8: Sample F: part of graphical representation of EDM with red boundary foreground pixels. Grey colour indicates increasing distance value.

Local maxima of EDM – the lightest areas in figure (Fig. 8) were considered as a centers of pore sections and the value of Euclidean distances there as radiuses of pore sections. In next step circles of such radiuses approximated these vacancies. Result of this approximation is pictured in figure (Fig. 9):

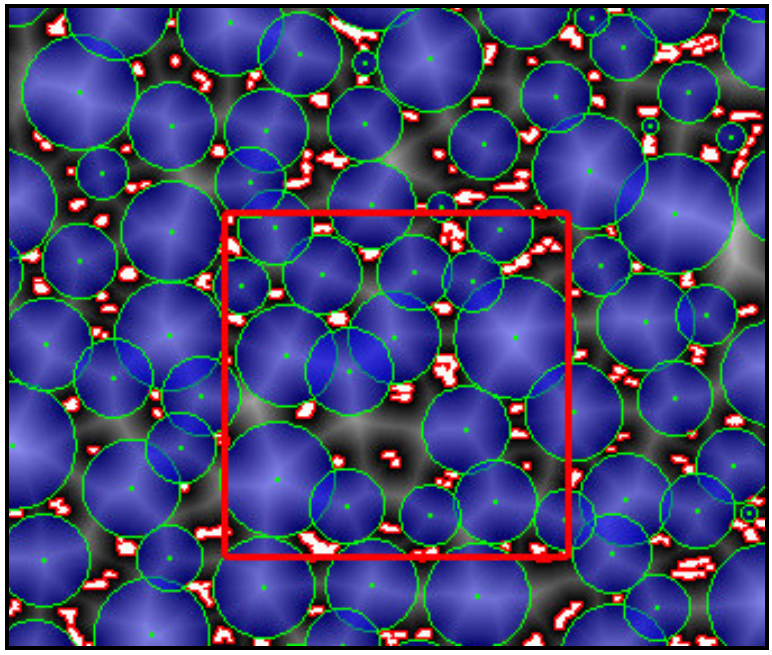

Fig. 9: Sample F: approximation of pore sections by circles. Red area is in detail in the figure (Fig. 10).

The problem of this approximation is possible overlapping of circles – shown in figure (Fig. 10a). To avoid bad computation, overlapping must removed manually (see the Appendix A II). Result of this process can be seen in figure (Fig. 10b).

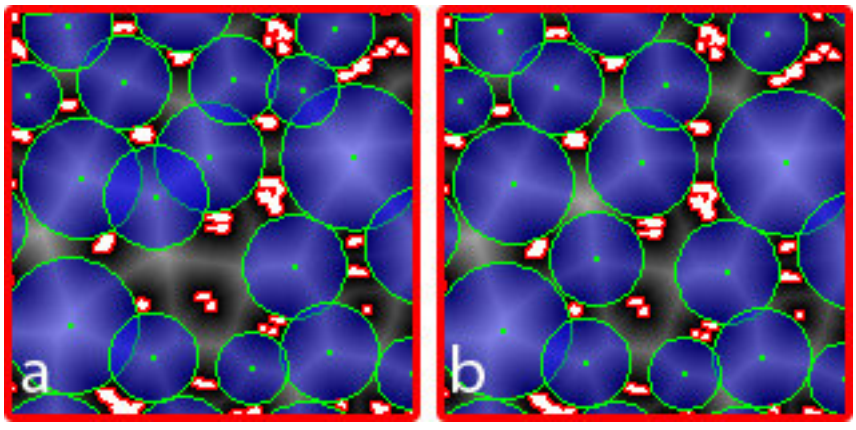

Fig. 10: Sample F: detail of approximation the EDM by circles. Overlapping circles in (7a) are filtered (7b).

The last step of image analysis is computation of the Voronoi tessellation, based on local maxima of EDM. Let $P = \{p_1, p_2, \ldots p_n\}$is a set of points in d-dimensional space $\boldsymbol{R}^d$

(d = 2 for our planar images). The Voronoi tessellation for P is the partitioning of the space which associates a region $V(p_i)$ with each generator p_i from P in such a way that all points in $V(p_i)$ are closer to p_i than to any other point in P. Equation (19) confirming this statement is shown below:

$$V(p_i) = \left\{ x \in \boldsymbol{R}^d, \left\| x - p_i \right\| \leq \left\| x - p_j \right\| \right\} \text{ for } i \neq j, \tag{19}$$

where $\left\| x - p_i \right\|$ is Euclidean distance. Voronoi tessellation based on local maxima of EDM (Fig. 9) is in the figure (Fig. 11). Finally the estimated areas of pore sections (computed by Voronoi tessellation) were exported and statistically evaluated.

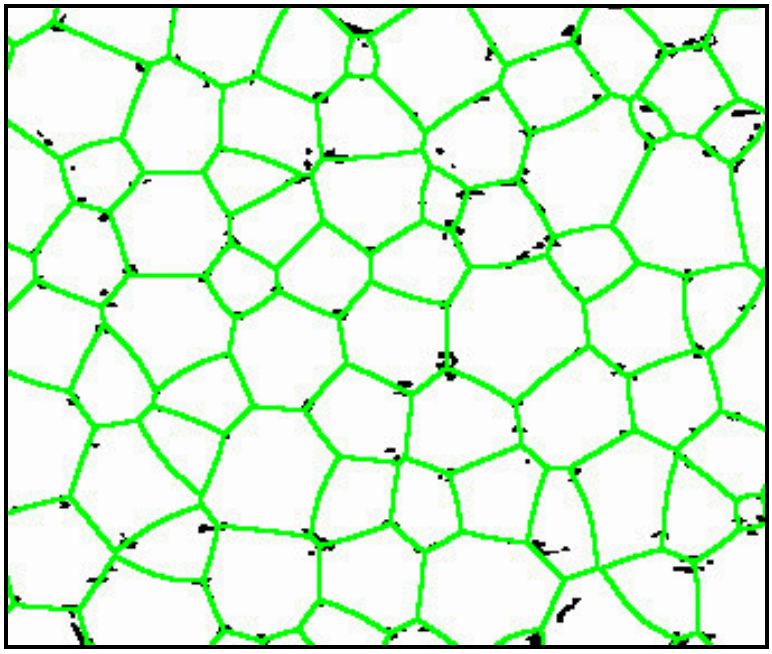

Fig. 11: Sample F: Voronoi tessellation based on local EDM maxima (green net) covering the original printed image.

4.2 Alternative methods of visualization

According to the task of this thesis the alternative methods of visualization pore structure were tested.

4.2.1 Direct scanning of foam

Direct scanning of foam was tested for its simplicity. A piece of foam without any previous preparation was scanned to get an image of structure on the surface. Part of planar section of scanned foam is shown in figure (Fig. 12). There are two circles there – the green

one represents area of polyurethane, where the recognizing of pore structure is possible, whereas the red circle shows the part of sample, where the recognizing of pore sections is impossible. In addition it is difficult to recognize surface pore sections from pore sections belongs to the deeper layers everywhere. Because of these two imperfections this method is unsatisfactory for obtaining image of planar section of any foam.

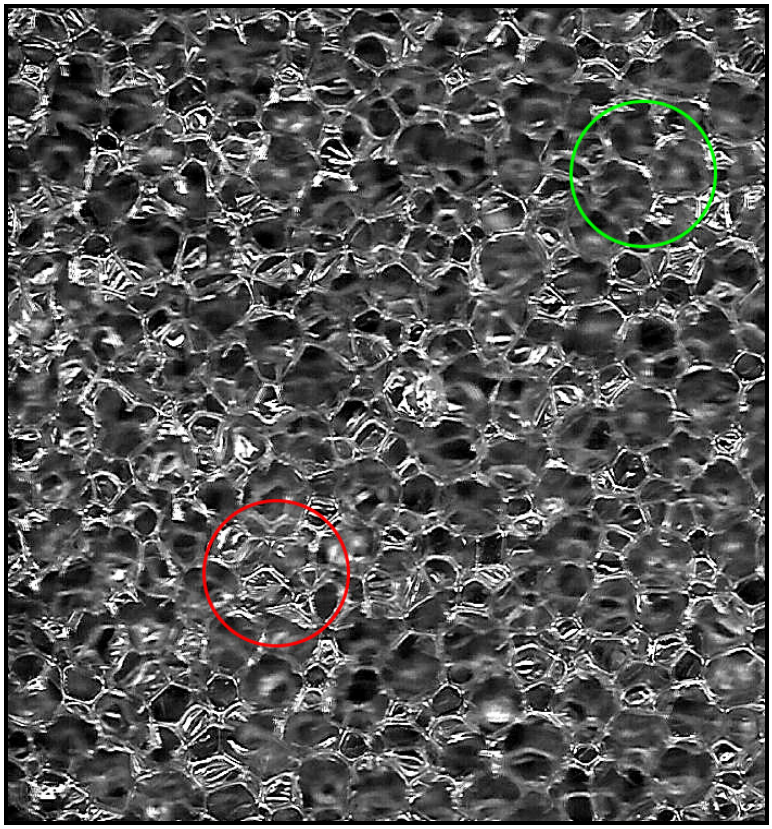

Fig. 12: Image of directly scanned surface of sample G.

4.2.2 Saturation of pores by water glass

This method was tested for development a technique able to give a cut of structure. Saturation of pores by any liquid and its transformation into solid state is way, how to get a tough structure capable of cutting. As a saturation liquid the 30 % water solution of water glass (Na_2SiO_3) was selected. Water glass – viscous liquid, widely used as a glue or as an bonding agent in metallurgy, was selected because of it low cost and good availability. This technique was based on presumption of water glass hardening described by chemical equation (20):

$$Me_2SiO_3 + H_2CO_3 \rightarrow Me_2CO_3 + H_2SiO_3\ (\text{gel } SiO_2 \cdot n\ H_2O), \qquad (20)$$

where Me can be any alkali metal.

The small pieces of foam were saturated and slowly heated to the temperature around 60-70 °C to speed curing reaction. Unfortunately after 12 hod of curing the samples were still soft. It is assumed that this failure was caused by low concentration of water glass – – heating process cured the water glass but evaporate the solvent. Evaporation of water was the cause of no saturation of most of pores.

For improvement of this method the usage of contrast and inert reinforcement was tested. As a reinforcing material the titanium dioxide and zinc white (also known as white pigments) were used. The samples of foam were saturated by paste made from water glass and pigments. Different concentrations of pigments were tested, but the result after curing was the same as in previous case.

4.2.3 Printing and scanning – alternative colours

It seems to be that this technique is the best from all of tested. For comparison with the validated colour (black stamping ink) the alternative ones were tested for printing. After testing of watercolour, alcoholic black felt tip and food colour it was recognized that the stamping ink is the best choice.

4.3 Evaluation of measurement

Data of pore section areas obtained by P&S was exported to MS Excel and arithmetical averages and standard deviations were calculated. The table (Tab. 3) sums up the estimated average pore section areas with standard deviations and radiuses of pore section calculated from average pore section areas with standard deviation.

Tab. 3: Calculated average pore section areas and radiuses of pore section from individual measurements.

Measurement	Average pore section areas *A* [px], average radiuses of pore sections *r* [px].									
	Sample A		Sample D		Sample E		Sample F		Sample G	
	A	*r*	*A*	*r*	*A*	*r*	*A*	*r*	*A*	*r*
1	1402	16,63	973	14,45	1131	14,06	1526	17,56	2159	19,78
2	1215	14,44	782	11,86	1332	16,75	1579	18,06	2253	20,82
3	1072	13,58	762	11,73	1191	15,58	1470	16,80	2263	21,96
4	1173	15,09	895	13,16	1374	16,60	1495	17,57	2137	21,17
5	1002	13,50	719	11,50	1368	16,68	1441	16,93	2238	21,17
6	982	13,36	725	11,75	1281	15,93	1402	17,36	2235	20,98
7	1048	13,11	715	10,62	1342	15,98	1380	16,12	2637	23,02
8	1074	14,01	760	11,48	1311	16,34	1228	15,79	2495	23,71
9	1086	14,32	845	12,21	1278	15,93	1396	16,54	2466	21,74
10	1054	13,55	702	10,51	1249	15,78	1306	15,76	2384	21,39
11	1160	14,63	755	11,68	1333	16,74	1295	15,03	2595	23,43
12	1032	13,27	704	10,93	1311	15,07	1253	15,27	2624	22,97
13	1058	13,50	687	11,12	1081	14,38	1461	16,67	2247	21,06
14	723	10,58	714	10,70	1165	15,85	1488	16,75	2651	24,50
15	920	12,51	758	11,33	1190	15,37	1333	15,64	2708	24,72
16	865	11,86	781	12,02	1048	14,66	1354	15,00	2563	24,33
17	980	12,85	696	10,95	1255	16,72	1385	16,40	2690	24,24
18	775	11,12	670	10,89	1148	14,85	1232	15,63	2732	24,63
19	881	11,99	711	10,57	1332	16,05	1290	15,36	2720	24,87
20	862	11,90	820	11,78	1336	17,28	1412	16,65	2294	22,31
21	788	11,85	874	13,00	1125	14,60	1234	14,99	2750	25,03
22	969	13,05	907	13,18	1002	13,85	1517	16,59	2779	23,84
23	825	11,59	927	12,73	1292	15,57	1544	17,18	2263	21,18
24	841	11,51	831	11,63	1107	13,98	1393	16,03	2415	22,09
25	1074	14,23	770	11,27	1342	16,50	1436	17,13	2651	23,61
26	973	14,19	810	11,81	1330	16,48	1299	16,31	2583	23,01
27	856	11,94	826	12,29	1319	16,16	1556	18,22	2776	24,67
28	1159	14,32	833	12,35	1187	14,54	1341	16,79	2872	25,06
29	1169	15,50	967	13,81	1156	14,26	1331	16,61	2635	23,60
30	-	-	842	12,43	1172	14,08	1475	17,29	2524	23,26
Total average	**1001**	**13,24**	**791**	**11,84**	**1239**	**15,60**	**1392**	**16,44**	**2511**	**22,93**
σ	151	1,38	84	0,97	103	0,97	101	0,87	215	1,52

4.4 Modeling of structure

Pore section areas are obtained by P&S analysis, but pore volumes are required. Pore volumes were estimated by computer simulation. The normal distribution of pore radiuses with some mean value **E***r* and standard deviation σ_r was assumed. About 6000 spheres with these parameters were generated. For each sphere a plane X with uniform distribution of distance in interval <0; **E***r* +3σ_r > from sphere centre was generated (note that **E***r* +3σ_r is the maximal sphere radius). If the random plane X intersects the sphere, section area was computed. The distribution of section areas of pores are known from experiment. The distribution of sphere sections is computed by simulation. The goal is to find such sphere parameters **E***r* and σ_r, to minimize sum of square deviations of experimental and simulated distributions.

Pore volume distribution is lognormal [9]. If the pore section radiuses have normal distribution, the distribution of pore volumes is not lognormal, but shape of our pore distribution is similar to lognormal. For not extremly big amount of measured pores it is easy to equate both these distributions.

4.4.1 Wicksell's problem

Planar cutting of porous media brings a several problems. For understanding the Wicksell's problem a model situation of porous material is shown in figure (Fig. 13) – spherical pores are distributed in volume of material randomly. An arbitrarily selected cutting plane intersects the pores in different positions. When the diameter of pore lies outside of cutting plane, the area of circle (originated by intersection) is smaller than the diameter of pore [27].

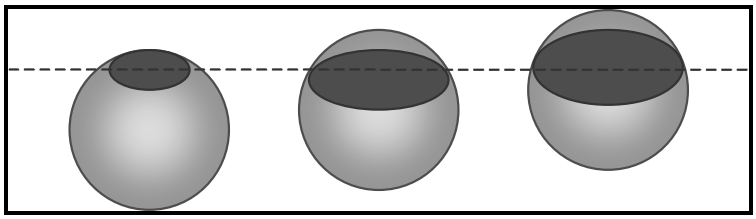

Fig. 13: Wicksell's problem [27].

The modelling have been carried out in MS Excel, by using macro computation. The VBA code of macro is shown in Appendix A III. The apperance of the Excel file is figured in (Fig. 14).

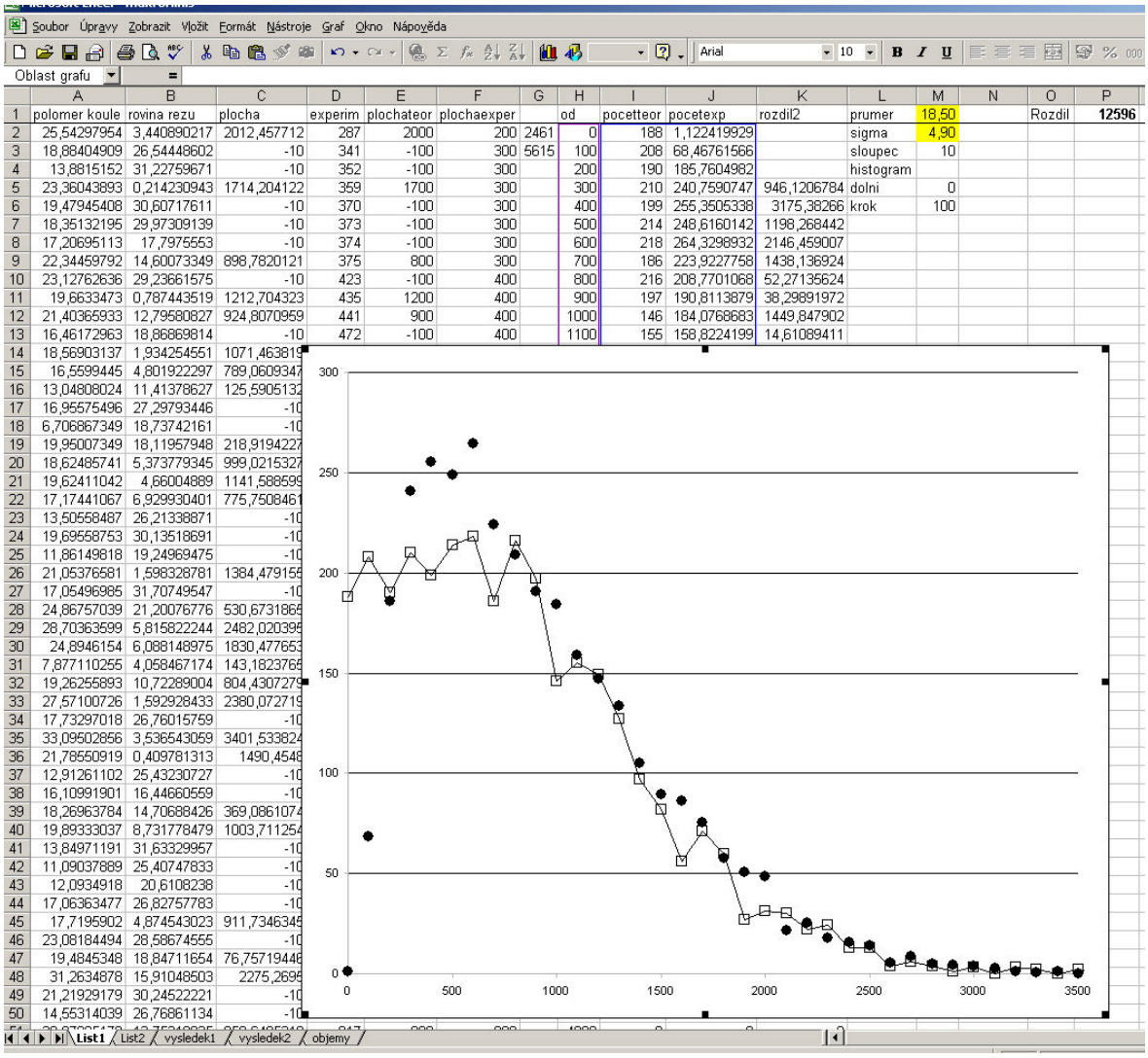

Fig. 14: Apperance of Excel file for modelling of structure.

In column A in figure (Fig. 14) the random radiuses r of pore sections are generated on the basis of values in cells yellow M1 and M2, which represents the average radius of pore section r and standard deviation σ_r.

Column B shows the data of random plane X. If the value in column B is smaller than value in column A (at the same row) the area of intersection is calculated in column C.

Column D includes mean pore section areas obtained by P&S. The data from columns C and D are rounded down to hundreds in columns E and F.

The interval of $\mathbf{E}A$ is written in column H.

Data in Columns I and J are calculated on basis of values in columns E, F and H – the amount of pore sections with areas from interval in column H are counted from columns E (theoretical) and column F (P&S), whereas column E coresponds with column I and column F coresponds with column J. The values in column J is standardized for amount of theoretical data. Finally the square of deviations of each row of columns I and J are calculated in column K. The graph in figure (Fig. 14) shows the comparison between theoretical prediction (connected squares) and obtained **E***A* (circles).

This model is based on change the values of average radius of pore section *r* (cell M1 in (Fig. 14)) and standard deviation σ_r (cell M2). The influence of changing these values to the shape of curve is shown in graphs from (Graph 1) to (

Graph *3*) where the movement of curves is demonstrated.. Small value of σ_r (e. g. in graph (Graph 1) in comparison with higher value σ_r and the same value of radius of pore section *r* (Graph 2) denotes the move of curve up – it is caused because the probability of intersection with generated sphere with such radius rises. The different scale of y-axis in all of these graphs are caused by standardization of experimental data to the amount of generated theoretical data.

Graph 1:Sample A: comparison of theoretical prediction of distribution (connected circles) and the experimental data for values r =18,5; σ = 2,5.

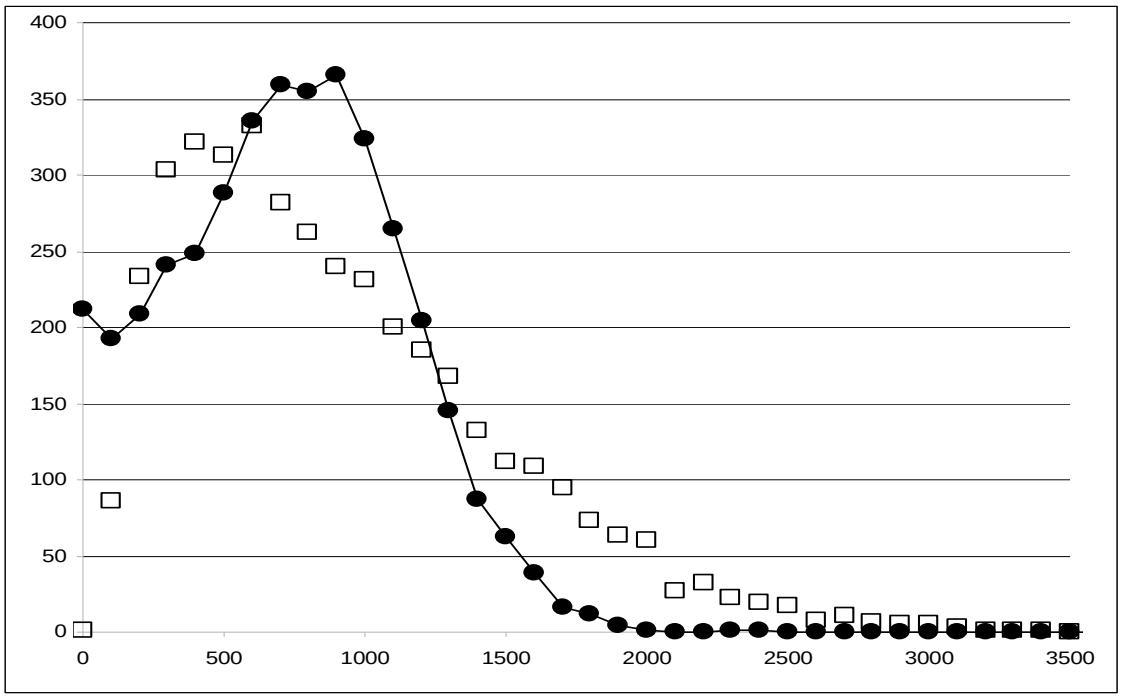

Graph 2: Sample A: comparison of theoretical prediction of distribution (connected circles) and the experimental data for values r =18,5; σ = 4,9.

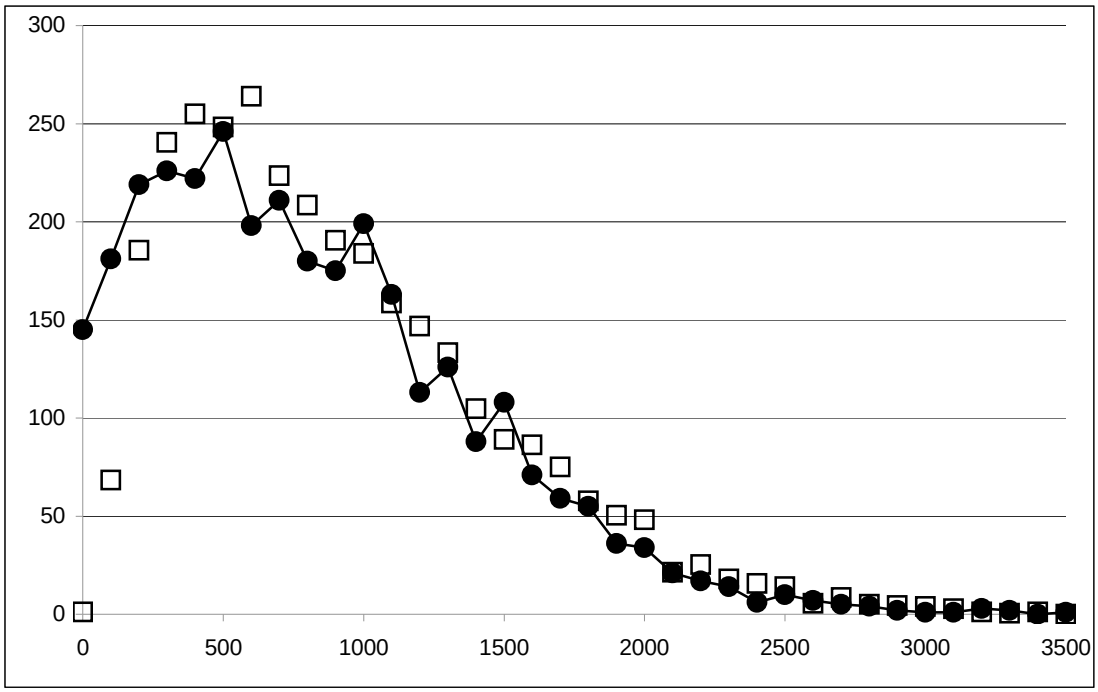

Graph 3: Sample A: comparison of theoretical prediction of distribution (connected circles) and the experimental data for values r =14; σ = 4,4.

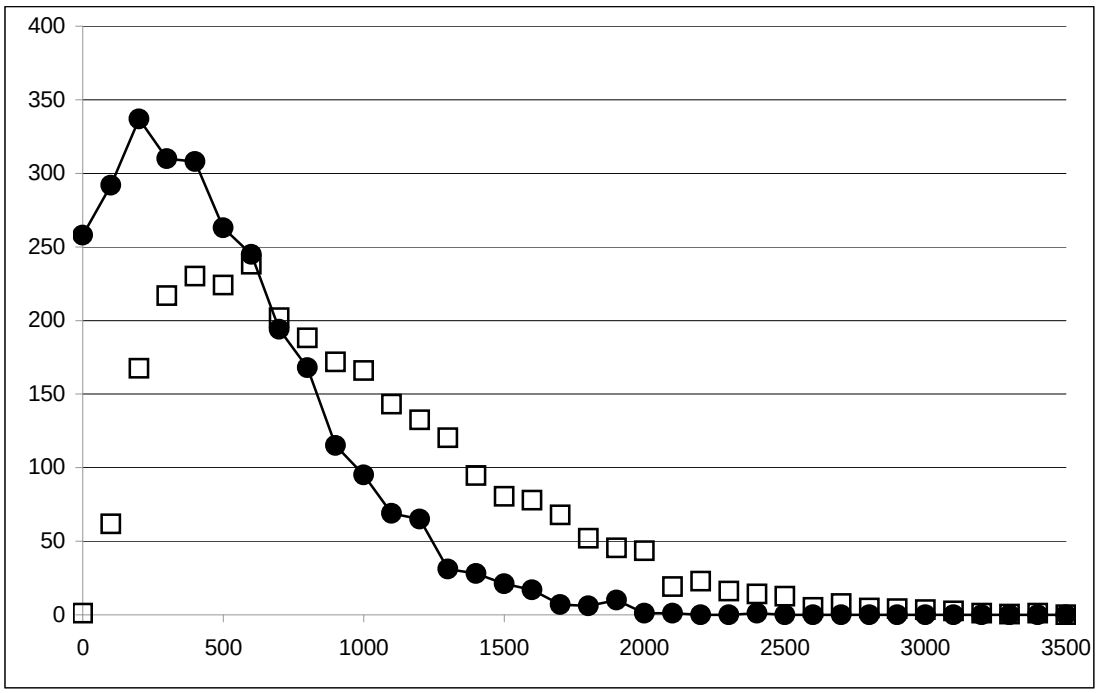

4.5 Acoustic properties

Measurement of acoustical properties has been carried out on the two-microphone impedance tube (Kundt's tube) Brüel&Kjaer. By this measurement the values of absorption coefficient α and reflection coefficient R have been found. Finally the relations between structure and acoustic properties have been described.

4.5.1 Equipment

Three-channel portable PULSE multi-analyzer Brüel&Kjaer, type 3560-B-030:

PULSE, shown in figure (Fig. 15), is portable apparatus for elaboration and analyzing of acoustic signals in real time. It works in frequency range from 0 Hz to 25,6 kHz. In combination with two-microphone impedance tube (Kundt's tube) Brüel&Kjaer allows to study absorption characteristics of materials [45].

Fig. 15: Three-channel portable PULSE multi-analyzer Brüel&Kjaer, type 3560-B-030 [45].

Two-microphone impedance tube Brüel&Kjaer:

This part of equipment, also known as Kundt's tube, pictured in figure (Fig. 16), is a standard tool used for determination of absorption coefficient α and reflection coefficient R of small samples. It consists of two tubes with diameters 100 mm and 29 mm for measurement in frequency range from 50 Hz to 1,6 kHz (bigger diameter) and from 500 Hz to 6,4 kHz. Measurement is based on decomposition of acoustic signal (generated by source) to incident and reflected part.

Aforementioned PULSE multi-analyzer performs analyzing of signal and with the help of auxiliary apparatuses – Amplifier of signal Brüel&Kjær type 2706 and computer with software BZ5050, the values of observed quantities are obtained. Arrangement of apparatuses for measurement are figured in figures (Fig. 17) and (Fig. 18).

Fig. 16: Two-microphone impedance tube Brüel&Kjaer [45].

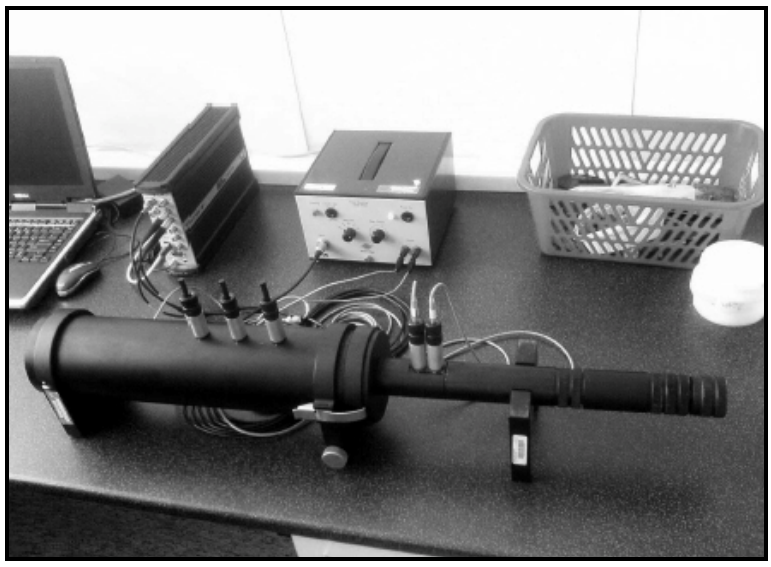

Fig. 17: Picture of connected aparatusses [46].

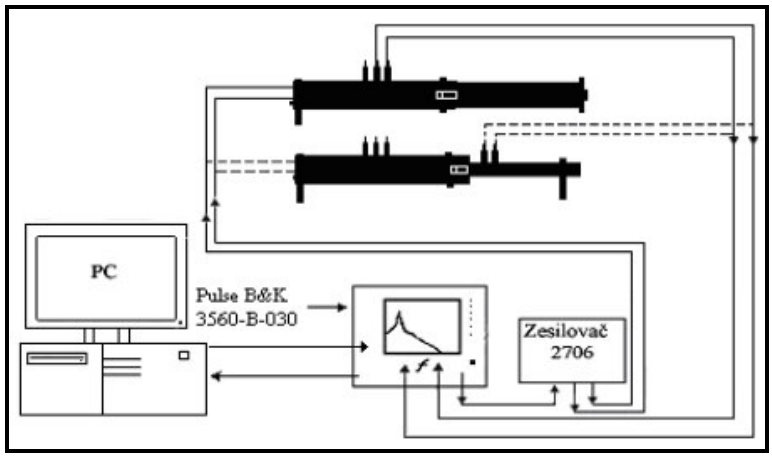

Fig. 18: Scheme of network (zesilovač is amplifier) [47].

4.5.2 Preparation of samples

With respect to the apparatus shape (tube) the samples with cylindrical shape had been prepared. Preparation of samples to the measurement was performed on the cold press, employing the circle cutting knives. The tools for sample preparation are figured in figure (Fig. 19).

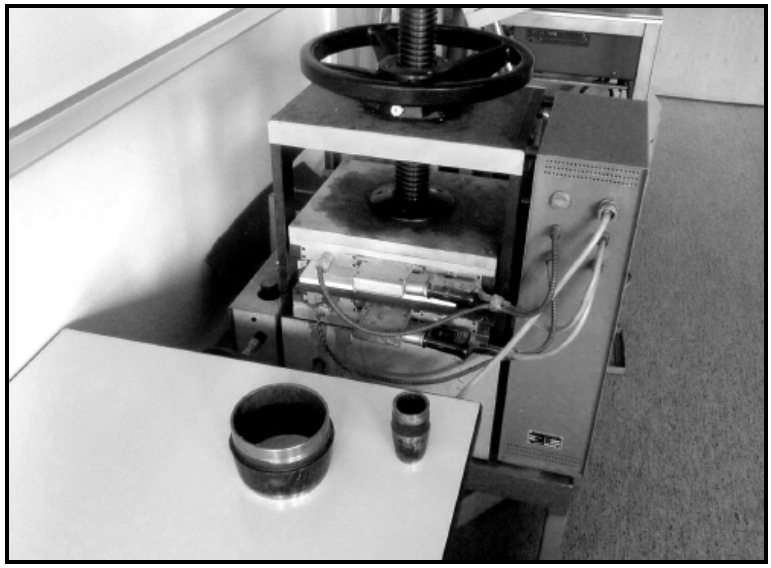

Fig. 19:Cold press anf cutting knives for sample preparation [46].

4.5.3 Measurement

At the beginning of measurement the calibration has been passed. The calibration is important for comparison of microphones signals – the reference sample has been measured with normal and interchanged positions of microphones.

Measurement of absorption coefficient α and reflection coefficient R has been performed for low frequencies (large tube with diameter 100 mm) and high frequencies (small tube with diameter 29 mm) separately. The measurement has been executed without air gap between the sample and the end of tube. After the insertion of sample to the Kundt's tube and adjust the holder of sample, the noise generator was started. This it was performed for all samples two times for both tubes. In addition two layers of the foam with the largest pores have been measured together. The thickness of samples is shown in table (Tab. 4):

Tab. 4: Thickness of samples.

Sample	Thickness [mm]
A	29,5
D	28,0
E	29,0
F	24,0
G	20,0

The measurement has been carried out at conditions summarized in table (Tab. 5). These values were preset in computer.

Tab. 5: Conditions of measurement.

Temperature of air [°C]:	20 °C
Air pressure [kPa]:	101,325
Relative humidity of air [%]:	30 %

4.5.4 Evaluation of measurement

After measurement the obtained data were processed. By using special software the curves of measured absorption coefficient α in low frequencies were connected with curves of α in high frequencies and made just one curve for one sample. The computed data – the values of α at measured frequencies were exported to MS Excel and graphs of α vs. frequency and R vs. frequency have been created.

5 RESULTS

5.1 Pore size estimation

Tab. 6: Transformed values from (Tab. 3) – average pore section areas [mm^2] and radiuses of pore sections [mm]. The 30th measurement of sample have been discarded.

Measurement	Average pore section areas *A* [mm^2], average radiuses of pore sections *r* [mm].									
	Sample A		Sample D		Sample E		Sample F		Sample G	
	A	*r*	*A*	*r*	*A*	*r*	*A*	*r*	*A*	*r*
1	0,53	0,32	0,37	0,28	0,43	0,27	0,58	0,34	0,82	0,39
2	0,46	0,28	0,30	0,23	0,51	0,33	0,60	0,35	0,86	0,41
3	0,41	0,26	0,29	0,23	0,45	0,30	0,56	0,33	0,86	0,43
4	0,45	0,29	0,34	0,26	0,52	0,32	0,57	0,34	0,81	0,41
5	0,38	0,26	0,27	0,22	0,52	0,33	0,55	0,33	0,85	0,41
6	0,37	0,26	0,28	0,23	0,49	0,31	0,53	0,34	0,85	0,41
7	0,40	0,26	0,27	0,21	0,51	0,31	0,52	0,31	1,00	0,45
8	0,41	0,27	0,29	0,22	0,50	0,32	0,47	0,31	0,95	0,46
9	0,41	0,28	0,32	0,24	0,49	0,31	0,53	0,32	0,94	0,42
10	0,40	0,26	0,27	0,20	0,47	0,31	0,50	0,31	0,91	0,42
11	0,44	0,29	0,29	0,23	0,51	0,33	0,49	0,29	0,99	0,46
12	0,39	0,26	0,27	0,21	0,50	0,29	0,48	0,30	1,00	0,45
13	0,40	0,26	0,26	0,22	0,41	0,28	0,56	0,33	0,85	0,41
14	0,27	0,21	0,27	0,21	0,44	0,31	0,57	0,33	1,01	0,48
15	0,35	0,24	0,29	0,22	0,45	0,30	0,51	0,30	1,03	0,48
16	0,33	0,23	0,30	0,23	0,40	0,29	0,51	0,29	0,97	0,47
17	0,37	0,25	0,26	0,21	0,48	0,33	0,53	0,32	1,02	0,47
18	0,29	0,22	0,25	0,21	0,44	0,29	0,47	0,30	1,04	0,48
19	0,34	0,23	0,27	0,21	0,51	0,31	0,49	0,30	1,03	0,48
20	0,33	0,23	0,31	0,23	0,51	0,34	0,54	0,32	0,87	0,44
21	0,30	0,23	0,33	0,25	0,43	0,28	0,47	0,29	1,05	0,49
22	0,37	0,25	0,34	0,26	0,38	0,27	0,58	0,32	1,06	0,46
23	0,31	0,23	0,35	0,25	0,49	0,30	0,59	0,34	0,86	0,41
24	0,32	0,22	0,32	0,23	0,42	0,27	0,53	0,31	0,92	0,43
25	0,41	0,28	0,29	0,22	0,51	0,32	0,55	0,33	1,01	0,46
26	0,37	0,28	0,31	0,23	0,51	0,32	0,49	0,32	0,98	0,45
27	0,33	0,23	0,31	0,24	0,50	0,32	0,59	0,36	1,06	0,48
28	0,44	0,28	0,32	0,24	0,45	0,28	0,51	0,33	1,09	0,49
29	0,44	0,30	0,37	0,27	0,44	0,28	0,51	0,32	1,00	0,46
30	-	-	0,32	0,24	0,45	0,27	0,56	0,34	0,96	0,45
Total average	**0,38**	**0,26**	**0,30**	**0,23**	**0,47**	**0,30**	**0,53**	**0,32**	**0,95**	**0,45**
σ	0,06	0,03	0,03	0,02	0,04	0,02	0,04	0,02	0,08	0,03

Estimated data of pore section areas and radiuses of pore sections, summarized in table (Tab. 3) have been obtained by P&S technique and consequent EDM analysis in SW Tessellation. The values in pixels cannot describe the real dimensions of samples. The data from table (Tab. 3) has been transformed to millimeters and summarized in table (Tab. 6).

5.2 Distribution curves

Distribution curves of pore section areas have been created from measured data gained by P&S and SW Tesselation. Graphs from (Graph 4) to (Graph 8) represents the distribution curves of pore section areas of samples. The dots in graphs represent an averages pore section sizes of each of six times scanned piece of foam. The curves show the total average and distribution curve of such material. In case of samples A, D and E it is obvious that these materials have a high amount of smaller pore sections. Samples F and G have more uniform distribution of pore section areas. The shapes of curves (mainly of sample F and G) are irregular because of small amount of measured data. Graph (Graph 9) represents the comparison of average distribution curves of samples.

Graph 4: Distribution curve of pore section areas – sample A.

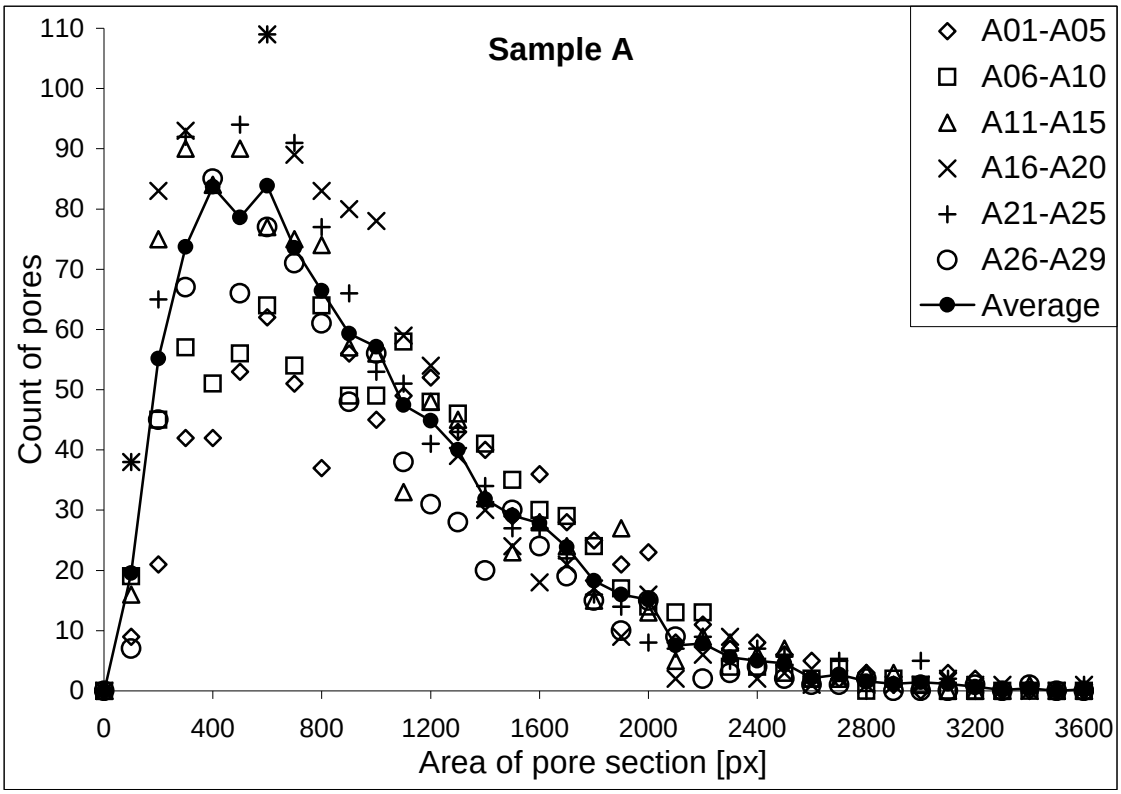

Graph 5: Distribution curve of pore section areas – sample D.

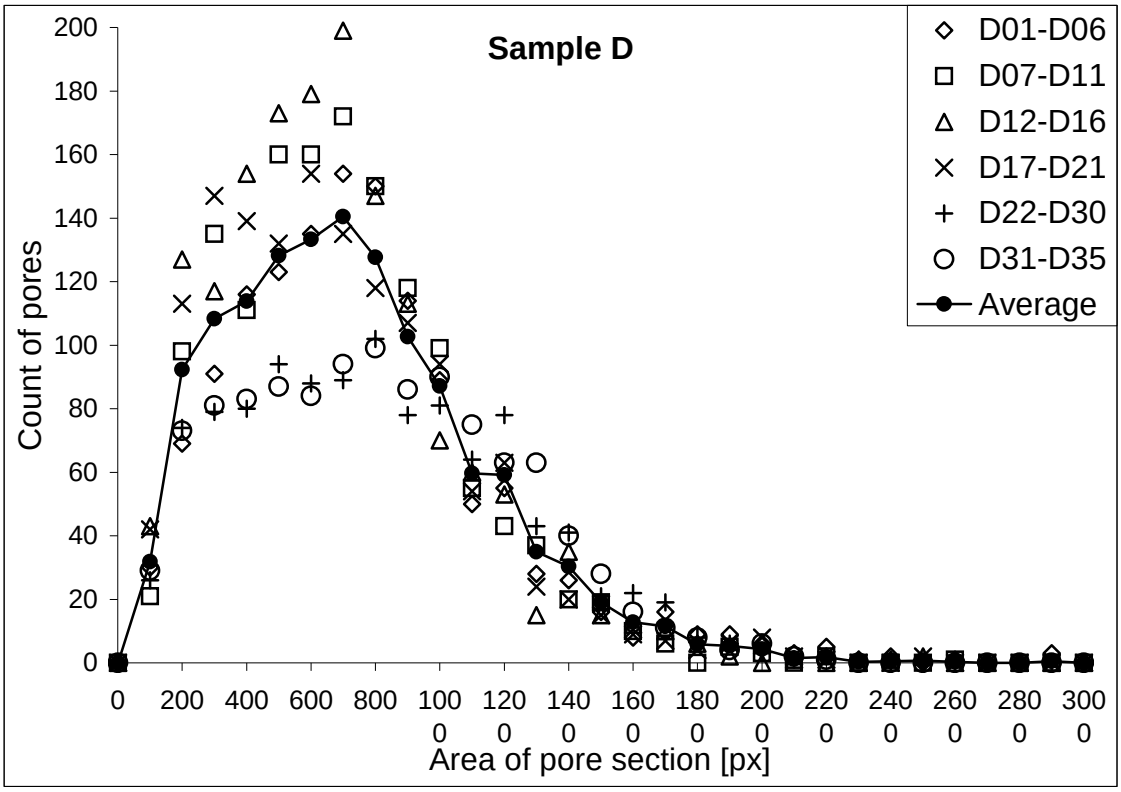

Graph 6: Distribution curve of pore section areas – sample E.

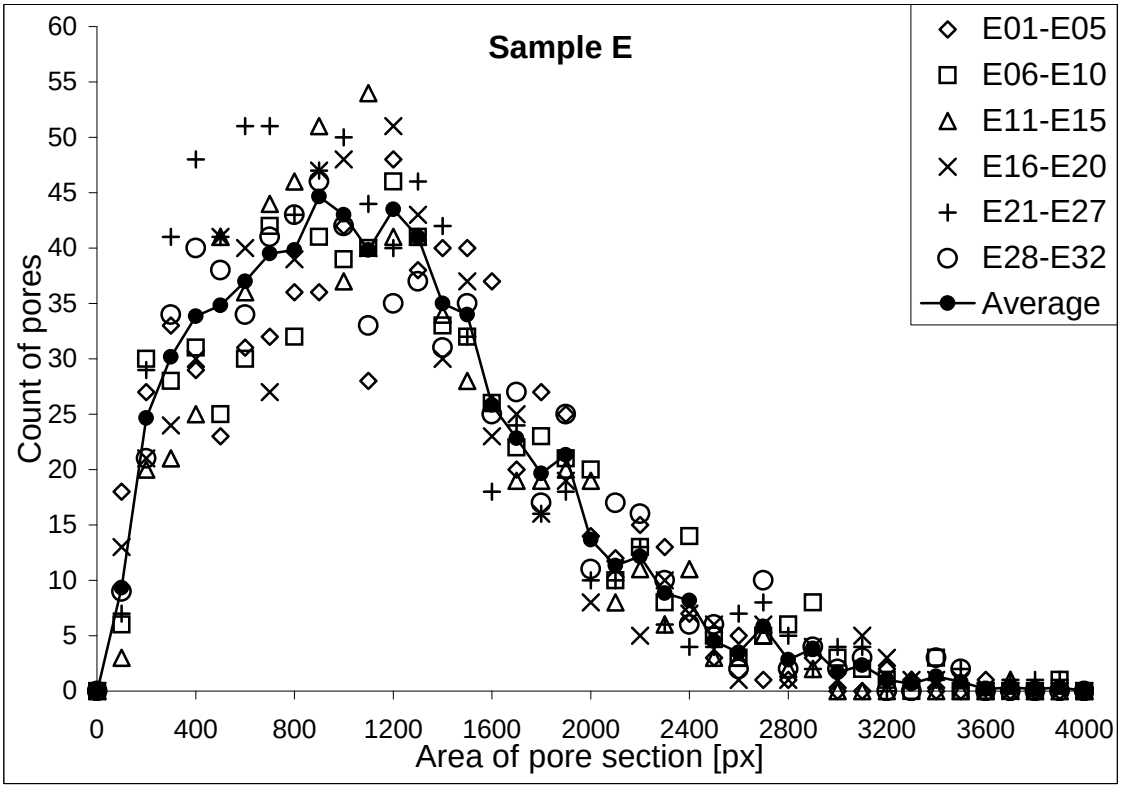

Graph 7: Distribution curve of pore section areas – sample F.

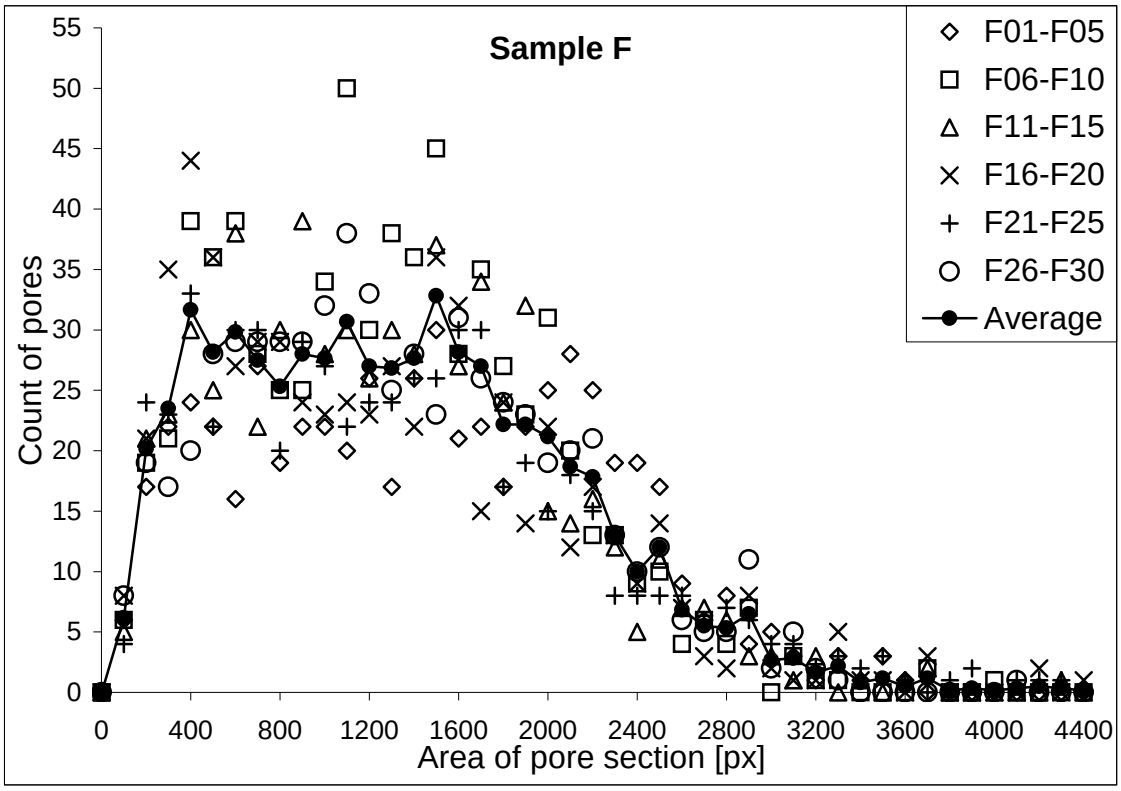

Graph 8: Distribution curve of pore section areas – sample G.

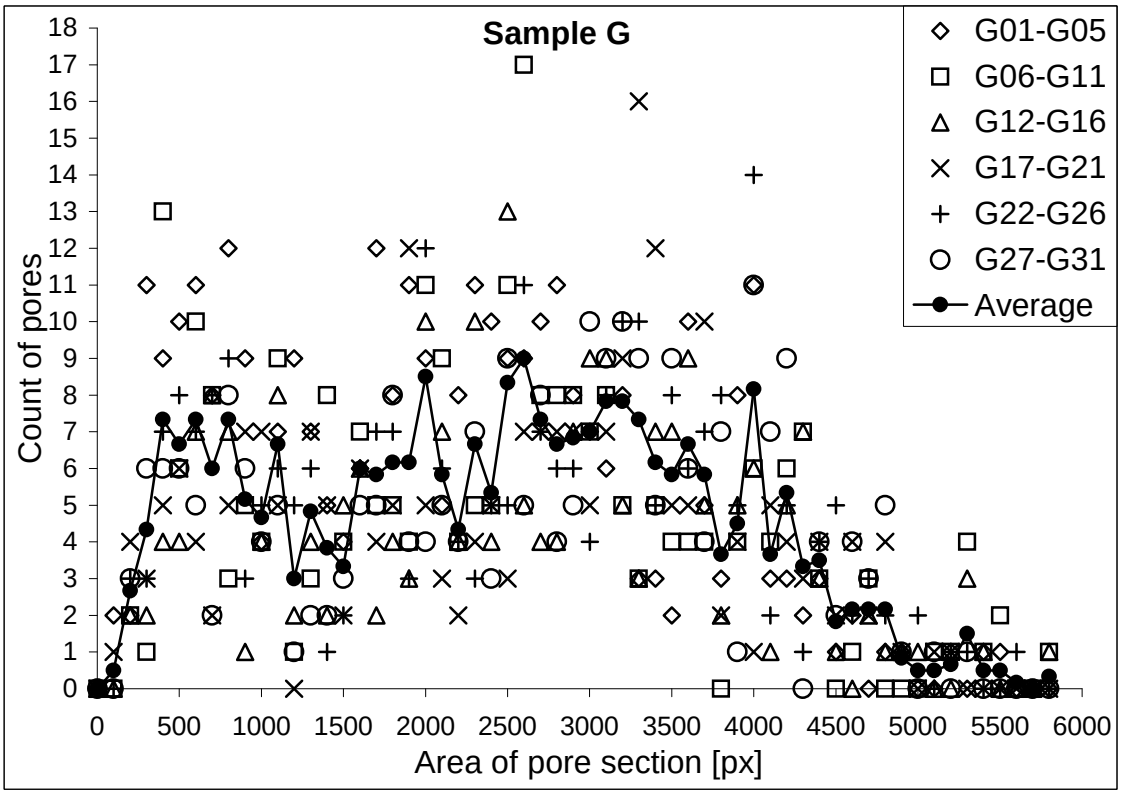

Graph 9: Comparison of average distribution curves of all samples.

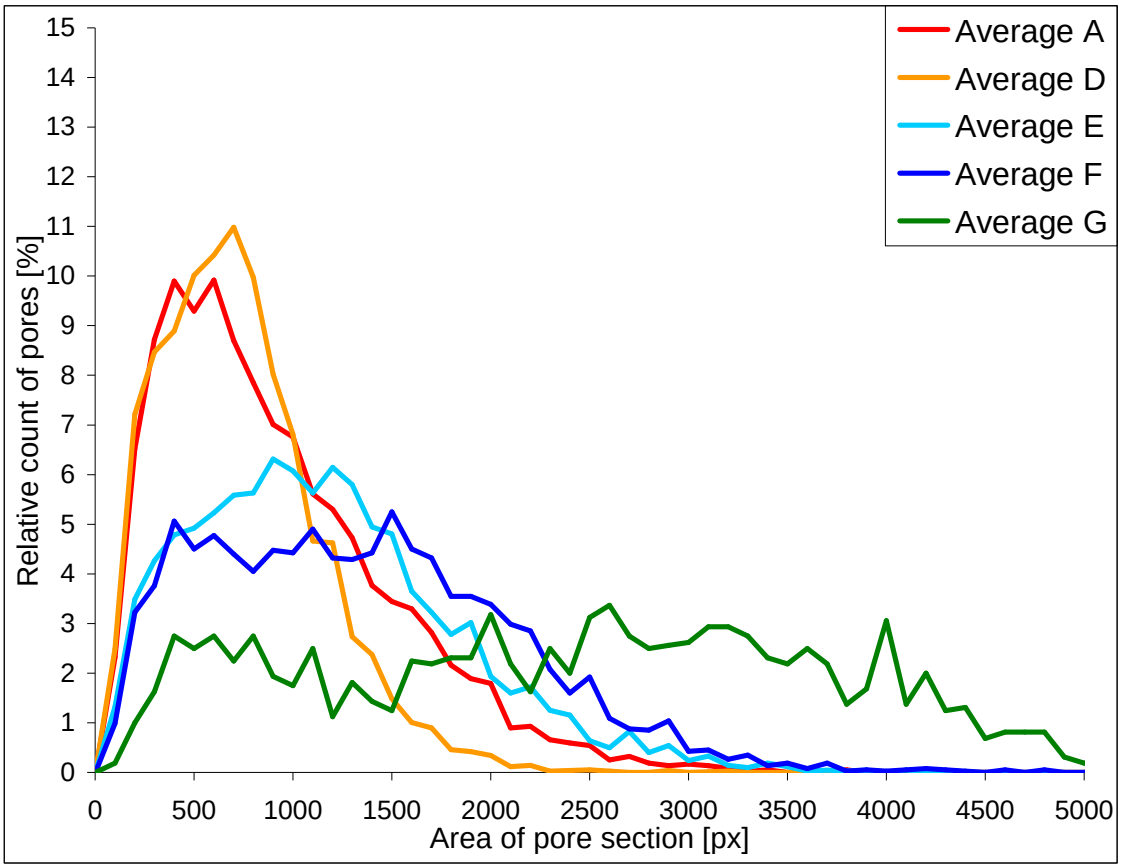

5.3 Pore volumes

The area of pore sections has been calculated in MS Excel. The values of r and σ_r has been estimated for the as small value of sum of squares Δ^2 as possible. Three different ways for calculation **E***V* were tested. The results in pixels are summarized in table (Tab. 7).

Tab. 7:Calculated r, σ_r and Δ^2 with minimal mean volumes.

SAMPLE	r [px]	σ_r	Δ^2	Mean volumes		
				E*V*$_1$ [px^3]	**E***V*$_2$ [px^3]	**E***V*$_3$ [px^3]
A	18,23	4,7	7868	25045	30153	41016
D	17,2	2,9	10754	21203	23058	30124
E	21,7	4,2	3907	48932	47607	59210
F	22,9	4,8	2791	42625	56975	70177
G	59,8	7,8	219	888590	932541	180992

Where **E***V*$_1$ has been calculated from the average r generated in Excel in column A (see figure (Fig. 14)) by using standard equation for sphere volume (V=4/3.π.r^3), **E***V*$_2$ is the average of sphere volumes calculated individually for each generated r in column A and **E***V*$_3$ were obtained from calculation by using equation for estimation of **E***V* from **E***A* according to the ASTM E 112 Standard (16). The values in pixels cannot describe the real dimensions of samples. The values of all **E***V* has been transformed to millimeters and summarized in table (Tab. 8).

Tab. 8:Calculated r, σ_r and Δ^2 with minimal mean volumes in millimeters..

SAMPLE	r [mm]	σ_r	Δ^2	Mean volumes		
				E*V*$_1$ [mm^3]	**E***V*$_2$ [mm^3]	**E***V*$_3$ [mm^3]
A	0,36	4,7	7868	0,187	0,225	0,306
D	0,34	2,9	10754	0,158	0,172	0,225
E	0,42	4,2	3907	0,320	0,355	0,442
F	0,45	4,8	2791	0,375	0,425	0,523
G	1,17	7,5	3904	6,628	6,956	1,350

It is obvious in table (Tab. 8) that the mean pore volumes **E***V* differ very strongly in dependence on used method. Note that all three methods exploit the same image data and difference is not evoked by difference in samples, method of visualization of image analysis. The table (Tab. 8) confirms premises used by ASTM E-112 Standard [40]. This

standard describes grain size by a number *G* corresponding with grain volume by relation $\mathbf{E}V \approx 2^G$. The one step difference in *G* corresponds with two times greater grains. The reason of this procedure is impossibility of exact measurement of grain size.

5.4 Acoustical characteristics

The acoustical quantities of absorbtion coefficient α and reflection coefficient *R* have been measured in frequency range 64-6400 Hz. The maximal values of these coefficients are summarized in table (Tab. 9).

Tab. 9: Maximal values of α and R of samples and the frequency of maximal noise absorption.

Sample	Thickness of sample [mm]	Density of sample [kg.m^{-3}]	Maximal values of α and *R* [-]				Corresponding *f* [Hz]	
			Global maximum		Local maximum		Global maximum	Local maximum
			α	*R*	α	*R*		
A	29,5	21,12	0,642	0,358	-	-	3296	-
D	28,0	22,60	0,706	0,294	-	-	3424	-
E	29,0	34,14	0,980	0,020	0,897	0,103	6400	2416
F	24,0	22,74	0,644	0,356	-	-	4792	-
G	20,0	23,70	0,704	0,296	-	-	4864	-
G – double	40,0	23,70	0,934	0,066	0,795	0,205	5352	1960

The noise absorption curves in whole measured range are shown in graphs (

Graph *10*) and (Graph 11). The absorption curves of samples A, D, F and G has the similar trend and each curve can be divided to two regions. At the lower frequencies (approximately up to 2500 Hz) the curves can be fitted by lines with the similar slope. It means that the dependence of α on frequency is almost linear. At higher frequencies the deviation from linear behaviour is observed. The curves pass the maximal value of α and then rest at the comparable value or decreases slightly. According to the table (Tab. 9), it is possible to state that maximal values of α denoting the maximal noise absorption ability of material are comparable for samples A and F and for samples D and G, whereas the maximal values are observed at different frequencies. It is obvious, that the higher density of foam compensate the smaller thickness.

The absorption curves of samples E and two layers of sample G are different. These curves increases faster because of greater slope and have the linear region in interval 0-1700 Hz approximately. In the second region we can find two maxima of α on the

curves. The first maxima of both curves are local – from these points the curves decreases dramatically to the local minima. The difference of value α between the local maxima and local minima is around 20 %. Consequently the α increases again to the global maxima. In the case of two layers of sample G the second fall at the end of measurement rage is observed too.

The reason of the different shape of absorption curves of samples F and two layers of sample G is not fully evident. In the first case it can be caused by distinctively different density of sample F. We are assuming the smaller pores inside the sample, which make difficult for air to pass through the sample. The measurement of resistance against air passing would confirm this statement. The In the case of two layers of sample G it is possible that the doubling of thickness has the similar effect as greater density.

Graph 10: Absorption coefficient of measured samples in range 64-6400 Hz.

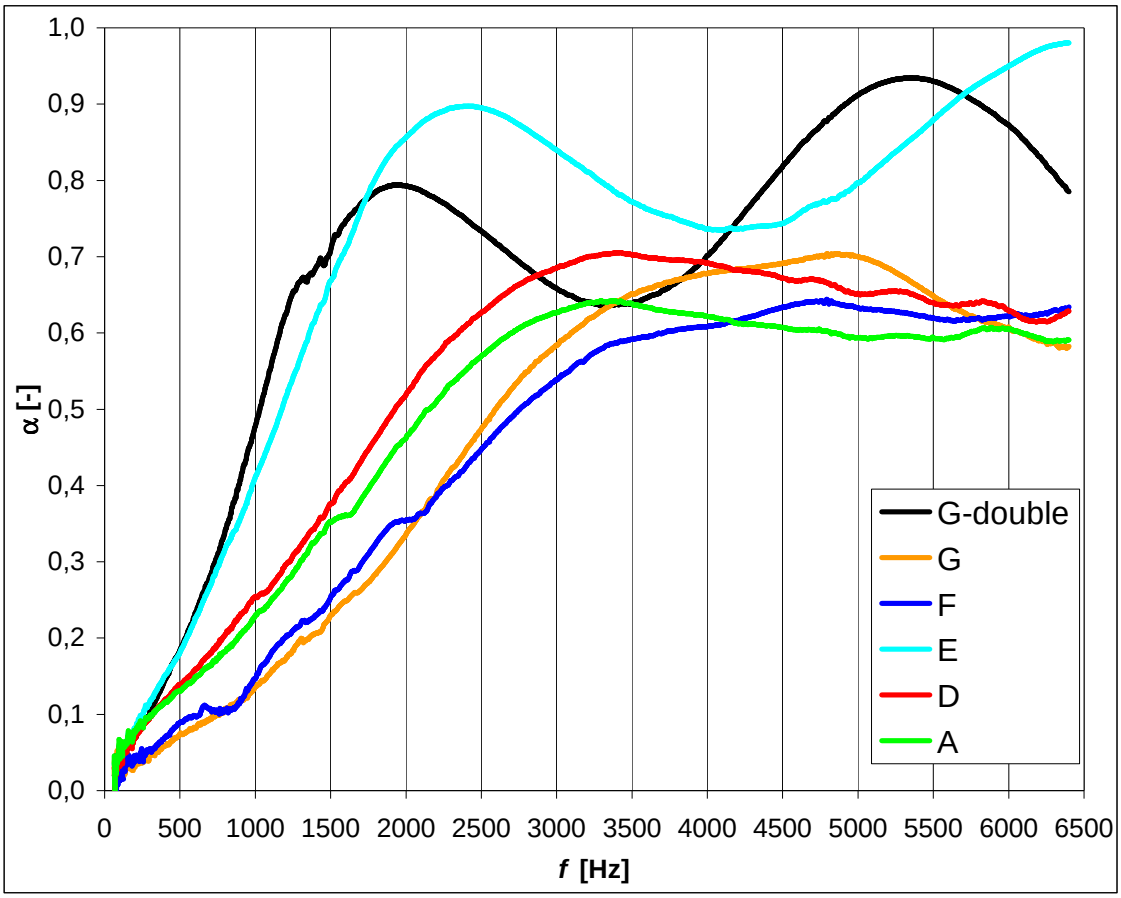

Graph 11: Reflection coefficient of measured samples in range 64-6400 Hz.

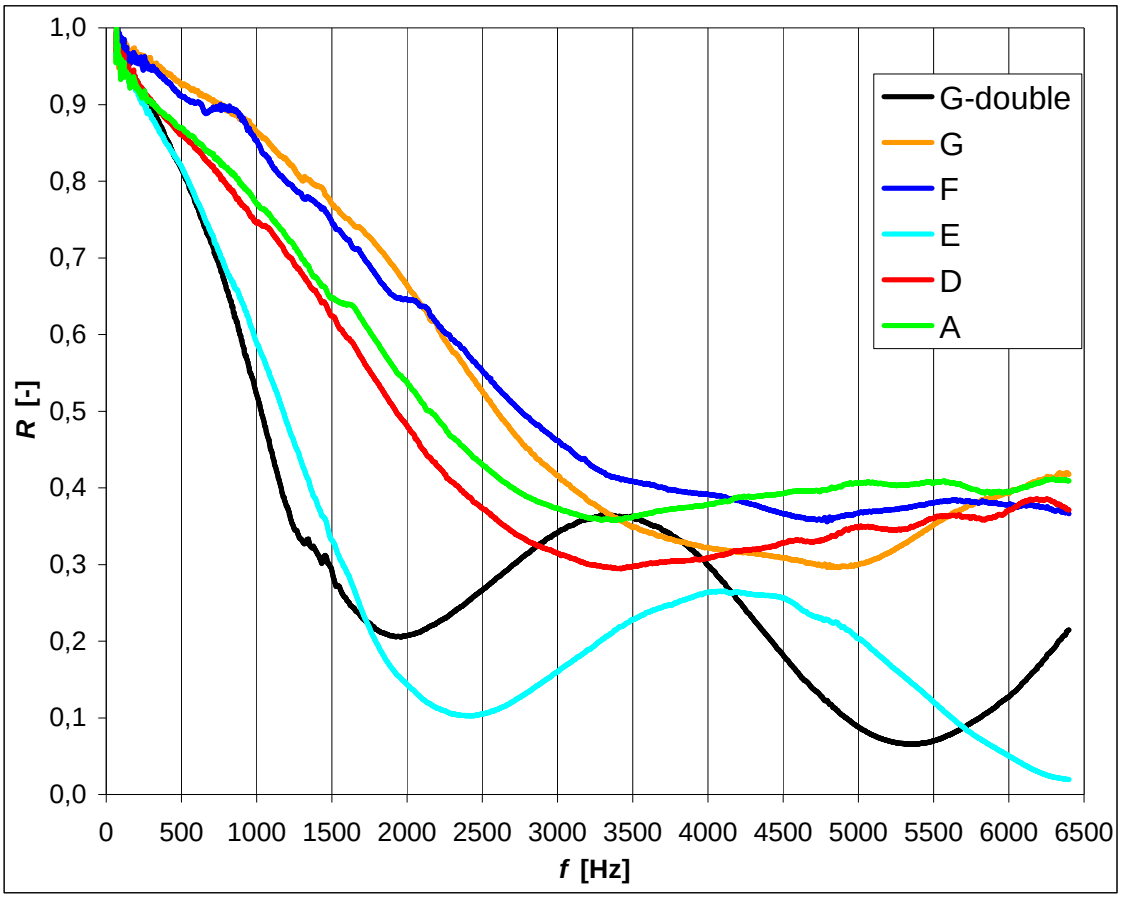

6 CONCLUSION

The "Printing and scanning" (P&S) method for visualization planar section of flexible polyurethane foams has been suggested. It is based on cover the printed area with stamping ink and print on the sheet of paper. The obtained image is transformed to the digital form by scanning. The main advantage of this method is its simplicity and low demandingness on equipment (only computer with scanner is required).

Alternative methods of visualization were tested. Unfortunately all of tested methods (direct scanning of foam, saturation of foam by water glass and usage of alternative colours for P&S) have not been successful.

Five samples of flexible polyurethane foam have been investigated to estimate their pore section areas. The images of planar sections of samples obtained by P&S technique were analyzed by using EDM method in SW Tessellation and sizes of pore sections and radiuses of inscribed circles were calculated. The results of this procedure are summarized in tables (Tab. 3) and (Tab. 6). According to these data the distribution of pore section areas have been calculated and the distribution curves of pore section areas shown in graphs from (Graph 4) to (Graph 9) have been created.

Obtained data of pore section areas have been transformed to mean volumes $\mathbf{E}V$ by using three different methods. $\mathbf{E}V_1$ has been calculated from the average r with normal distribution, generated in Excel by using standard equation for sphere volume ($V=4/3.\pi.r^3$), $\mathbf{E}V_2$ has been calculated on the basis of the average of sphere volumes calculated individually for each generated r with normal distribution and $\mathbf{E}V_3$ were obtained from calculation by using equation for estimation of $\mathbf{E}V$ from $\mathbf{E}A$ according to the ASTM E 112 Standard equation (16). The comparison of these values is in the tables (Tab. 7) and (Tab. 8).

Finally the acoustical properties of samples have been determined. The acoustical properties are characterized by absorption coefficient α and reflection coefficient R. Their dependency on frequency of sound is figured in graphs (

Graph *10*) and (Graph 11) and maximal values of measured quantities are summarized in table (Tab. 9). The results shows that absorption ability of foam is affected by density and thickness of layer. The dependency of absorption coefficient a on pore size have not been proved.

BIBLIOGRAPHY

[1] KLOUDA, P.: *Fyzikální chemie*. 1st ed. Ostrava: Pavel Klouda, **1997**. 179 pp. ISBN: 80-902155-2-1

[2] BERNAT, P.: A*kustika, vznik a šíření zvuku, frekvenční analýza a syntéza, sluchový vjem zvukového signálu*. [online]. **2008**. [cit. 2009-05-01]. Available at: <http://home.vsb.cz/petr.bernat/texty/varhany/anatomie/pistaly_akustika.htm>

[3] HALLIDAY, D., RESNICK, R. WALKER, J.: *Fyzika, Vol. 2: Mechanika – – Termodynamika*. 1st ed. Brno: VUTIUM, **2006**. pp. 439-440. ISBN: 80-214-1868-0

[4] MIŠUN, V.: *Vibrace a hluk*. 1st ed. Brno: FS VUT, **1998**. ISBN 80-214-1262-3

[5] FOJTŮ, D.: *Zvukově a tepelně izolační materiály pro aplikace ve stavebnictví*. Zlín, **2008**. 194 pp. Doctoral thesis. Tomas Bata University in Zlín. Faculty of Technology. Department of Physics and Materials Engineering. Supervisor: Lubomír Lapčík

[6] GONG, L., KYRIAKIDES, S., JANG, W.-Y.: Compressive response of open-cell foams. Part I: Morphology and elastic properties. *International Journal of Solids and Structures*. **2005**. 42(5-6). pp. 1355-1379

[7] GOSSELIN, R., RODRIGUE, D.: Cell morphology analysis of high density polymer foams. *Polymer Testing*. **2005**. 24(8). pp. 1027-1035

[8] LU, T.J., CHEN, F., HE, D.P.: Sound absorption of cellular metals with semiopen cells. *Journal of the Acoustical Society of America*. **2000**. 108(4). pp 1697-1709

[9] PISPOLA, G., HOROSHENKOV, K.V., KHAN, A.: Comparison of two modeling approaches for highly heterogeneous porous media. *Journal of the Acoustical Society of America*. **2007**. 121(2). pp 961-6

[10] MILLS, N.J.: *Polymer foams handbook - Engineering and Biomechanics Applications and Design Guide*. Elsevier Inc., **2007**. ISBN: 978-0-7506-8069-1

[11] SAXL, I., PONÍŽIL, P.: Grain size estimation: w–s diagram. *Materials Characterization*. **2001**. 46(2-3). pp. 113-118

[12] SAXL I., PONÍŽIL, P., SÜLLEIOVÁ K.: Grain size estimation in anisotropic materials. *Material Science Forum 482*. **2005**. pp. 239-242. [ISSN: 0255-5476, ISBN: 0-87849-964-4]

[13] MARK, H.F.: *Encyclopedia of Polymer Science and Technology, 12 Volume Set*. John Wiley & Sons, Inc., **2005**. ISBN: 978-0-471-27507-7

[14] MLEZIVA, J., ŠŇUPÁREK, J.: *Polymery – výroba, struktura, vlastnosti a použití*. 2nd ed., Prague: Sobotáles, **2002**. ISBN 80-85920-72-7

[15] Molitan JANA. [online]. [cit. 2009-05-11]. Available at: <http://www.molitan-jana.cz/produkty/molitan/>

[16] RYSZKOWSKA, J.: Quantitative image analysis of polyurethane/carbon nanotube composite micostructures. *Materials Characterization*. In press

[17] SALIBA, C.,CH. et al.: Effect of the incorporation of a novel natural inorganic short fiber on the properties of polyurethane composites. *Polymer Testing*. **2005**. 24(7). pp. 819-824

[18] JUŘIČKA, M.: *Materiály pro tlumení hluku a vibrací v leteckém průmyslu na bázi polyuretanů.* Zlín, **2008**. 167 pp. Doctoral thesis. Tomas Bata University in Zlín. Faculty of Technology. Department of Physics and Materials Engineering. Supervisor: Lubomír Lapčík

[19] BENEŠ, V.: *Stereologie a výběr*. [online]. **1998**. [cit. 2009-05-09]. Available at: <http://www.statspol.cz/robust/1998_benes_98.pdf>

[20] BUSCHOW, K.,H.,J. et al.: *Encyclopedia of Materials – Science and Technology, Volumes 1-11*. Elsevier Inc., **2001**. ISBN 978-0-08-052358-3

[21] PONÍŽIL, P.: Pore size estimation in open pores foams. *Macro 2008, International Conference on Polymeric Materials*. Taipei, June 29- July 4, **2008**

[22] FOTIADIS, D., FREDERIX, P.,L.,T.,M., ENGEL, A.: *Cell Biology – chapter 32*: *Atomic Force Microscopy in Biology*. 3rd ed. Elsevier Inc., **2006**

[23] LESLIE, W.,C., HORNBOGEN, E.: *Physical Metallurgy – chapter 17*: *Physical Metallurgy of Steels* . 4th ed. Elsevier Inc., **1996**

[24] CHEREMISINOFF, N.,P.: *Polymer characterization – chapter 3*: *Microscopy for polymer characterization*. Elsevier Inc., **1996**. ISBN: 978-0-8155-1403-9

[25] PELZBAUER, Z.: *Morfologie a mikroskopie polymerů V: Základy fyziky pevných polymerů*. POUCHLÝ, J., LEDNICKÝ, F., RAAB, M. Prague: Czechoslovakian Academy of Sciende, Department of Macromolecular Chemistry, **1987**

[26] TRAN, T., CAUDILL, M.: Using computer tomography and digital image processing techniques to measure blow molded objects. *ANTEC 1998 Plastics: Plastics on My Mind, Volume 3: Special Areas*. **1998**

[27] GALETKA, M.: *Strukturní analýza 3D pěny z rovinných řezů*. Zlín, **2008**. 49 pp. Bachelor thesis. Tomas Bata University in Zlín. Faculty of Technology. Department of Physics and Materials Engineering. Supervisor: Petr Ponížil

[28] SHEN, H., NUTT, S., HULL, D.: Direct observation and measurement of fiber architecture in short fiber-polymer composite foam through micro-CT imaging. Composites Science and Technology. **2004**. 64(13-14). pp. 2113-2120

[29] BERNAL, J.,L.,P., BELLO, M.,A.: Fractal geometry and mercury porosimetry: Comparison and application of proposed models on building stones. *Applied Surface Science*. **2001**. 185(1-2). pp. 99-107

[30] MA, Z., et al.: New developments in particle characterization by laser diffraction: size and shape. *Powder Technology*. **2000**. 111(1-2). pp. 66-78

[31] REDENBACH, C.: Microstructure models for cellular materials. *Computational Materials Science*. **2009**. 44(4). pp.1397-1407

[32] PONÍŽIL, P.: *Prostorové teselace – teze k rigorózní zkoušce*. Zlín, **1998**. 39 pp. University of technology Brno. Faculty of Technology in Zlín. Department of Physics and Materials Engeneering. Supervisor: Ivan Saxl

[33] ČERMÁK, R.: *Rovinné teselace jako model růstu* sférolitů. Zlín, **2001**. 92 pp. Master thesis. Tomas Bata University in Zlín. Faculty of Technology. Department of Physics and Materials Engineering. Supervisor: Petr Ponížil

[34] WARREN, J.E., ROOT, P.J: The Behavior of Naturally Fractured Reservoirs. *Society of Petroleum Engineers journal*.**1963**. 3. pp. 245-255

[35] OLNY, X., BOUTIN, C.: Acoustic wave propagation in double porosity media. *Journal of the Acoustical Society of America*. **2003**. 114(1). pp. 73-89

[36] SAMARDZIOSKA, T., POPOV, V.: Numerical comparison of the equivalent continuum, non-homogeneous and dual porosity models for flow and transport in fractured porous media. *Advances in Water Resources*. **2005**. 28(3). pp. *235-255*

[37] *Zpracovatelské vlastnosti textilních vláken*. Education text of Technical Universtiy of Liberec. Faculty of textile engineering. [online]. **2005**. [cit. 2009-05-09]. Available at: <http://www.ft.vslib.cz/depart/ktm/files/20060106/zvt_p_4.pdf>

[38] DANIELSSON, P.,E.: Euclidean distance mapping. *Computer Graphics and Image processing*. **1980**. 14. pp. 227-248

[39] WONG, H.,S., BUENFELD, N.,R.: Euclidean Distance Mapping for computing microstructural gradients at interfaces in composite materials. *Cement and Concrete Research*. **2006**. 36(6). pp. 1091-1097

[40] ASTM E 112. **1996** Standard Methods for Determining Average Grain Size

[41] *The Propagation of sound*. [online]. [cit. 2009-05-09]. Available at: <http://www.jhu.edu/~virtlab/ray/acoustic.htm>

[42] ŠŤASTNÍK, S., ZACH, J.: *Stavební akustika a zvukoizolační materiály*. Brno: CERM, **2002**. ISBN 80-214-2117-7

[43] Picture: Sound and impediment. [online]. [cit. 2009-05-09]. Available at: <http://www.mecart.com/modulars-studios/images/reflecabstransm.jpg>

[44] LAPČÍK, L., RAAB, M.: *Nauka o materiálech II*. Zlín: Univerzita Tomáše Bati ve Zlíně, Fakulta technologická, **2004**. 133 pp. ISBN 80-7318-229-7

[45] *Vybavení - přístroje umístěné na ústavu*. Tomas Bata University in Zlín. Faculty of Technology. Department of Physics and Materials Engineering. [online]. [cit. 2009-05-09]. Available at: <http://www.ft.utb.cz/czech/ufmi/vybaveni.html>

[46] URBAN, V.: *Studium vlivu struktury materiálu na jeho vibroakustické vlastnosti*. Zlín: **2008**. 93 pp. Master thesis. Tomas Bata University in Zlín. Faculty of Technology. Department of Physics and Materials Engineering. Supervisor: Martin Vašina

[47] STRUHAŘOVÁ, V.: *Polyuretany a jejich využití v technické akustice*. Zlín: **2008**. 60 pp. Bachelor thesis. Tomas Bata University in Zlín. Faculty of Technology. Department of Physics and Materials Engineering. Supervisor: Martin Juřička

LIST OF SYMBOLS AND ABBREVIATIONS

Symbol	Dimension	Meaning
A, A_{fm}, A_{fp}	[m]	Area, area of micro-porous scale, area of meso-porous scale.
AFM		Atomic force microscopy.
B, dB		Dimension of acoustic level.
b_{pq}		Mark of pixel in Euclidean Distance Map.
c	[m.s^{-1}]	Velocity of acoustic wave.
C`	[-]	Constant of equation for calculation of pore volume.
CCD		Charge-coupled device (chip).
CT		Computer tomography.
d	[m] or [-]	Diameter of circle profile or dimension.
d_{ij}	[px]	Euclidean distance.
D, D_{ϕ}	[m]	Diameter of pore. Average diameter of pore.
DP		Double porosity.
dpi		Dots per inch.
E, E_A	[J]	Acoustical energy, absorbed acoustical energy.
E*A*, **E***D*, **E***V*, **E***r*	[m^2], [m], [m^3], [m]	Mean area, mean diameter, mean volume, mean radius of pore.
EDM		Euclidean distance map.
e. g.		Exempli gratia.
et al.		Et alii.
etc.		Et cetera.
EVA		Ethylene-vinyl acetate copolymer.

Symbol	Dimension	Meaning
f	[Hz]	Frequency.
F	[N]	Force.
F_{BVC}		Biot viscosity correction function.
G		Exponent depending on pore volumes.
I	[W.m^{-2}]	Acoustic intensity.
I		Mean size of acoustic intensity.
I_0, I_1		Modified Bessel functions.
L		Acoustic level.
lm, lp		Micro-porous scale, meso-porous scale.
Me		Alkali metal.
OM		Optical microscopy.
p	[Pa] or [-]	Acoustic pressure or row in EDM.
p_0	[Pa]	Amplitude of acoustic pressure.
P	[W] or [-]	Acoustic power or set of points (Voronoi tessellation).
P_1, P_2	[W]	Acoustic power of source, acoustic power after transmission.
p_1, p_2, p_n		Points of set P.
p_i		Generator (Voronoi tessellation).
P&S		Printing and scanning technique.
PDF $f(r)$		Probability density function as a function of radius.
PE		Polyethylene.

Symbol	Dimension	Meaning
PP		Polypropylene.
PPO-PS		Polypropylene oxid, blend with PS.
PS		Polystyrene.
PUR		Polyurethane.
PVC		Polyvinylchloride.
PVT		Poisson-Voronoi tessellation.
px		Pixel.
q		Column in EDM.
RTG		X-ray.
s	[m]	Trajectory.
SEM		Scanning electron microscopy.
SW		Software.
t	[s]	Time.
T	[s]	Period.
T_B	[-]	Parameter of F_{BVC}.
TEM		Transmission electron microscopy.
v	[m.s^{-1}]	Velocity of particles oscilation.
VBA		Visual Basic.
r	[m]	Radius of pore.
R	[-]	Reflection coefficient, space of Voronoi tessellation.
R, R`		Radicals.
$V(p_i)$		Region of Voronoi tessellation.

Symbol	Dimension	Meaning
x		Position in EDM.
X		Cutting plane
X, X_0		Compared value, reference value.
Z	[N.s.m^{-3}]	Specific acoustic impedance.
α	[-]	Absorption coefficient.
Δ^2		Sum of squares.
Φ	[°]	Angle.
η	[Pa.s]	Dynamic viscosity of air.
κ	[m^3]	Parameter of F_{BVC}.
λ	[m]	Wavelength.
ξ	[-]	Transmission loss coefficient.
π		Pi.
ρ, ρ_0	[kg.m^{-3}]	Density, equilibrium density of air.
σ		Standard deviation.
Ψ_{db}, Ψ_m, Ψ_p	[Pa.s.m^{-2}]	Total flow resistivity, flow resistivity of micro-scale, flow resistivity of meso-scale.
ω	[s^{-1}]	Angular frequency.
Ω_{db}, Ω_m, Ω_p	[-]	Total open porosity, open porosity of micro-scale, open porosity of meso-scale.

LIST OF PICTURES

LIST OF TABLES

LIST OF GRAPHS

LIST OF APPENDICES

APPENDIX A I: SW TESSELLATION – APPERANCE

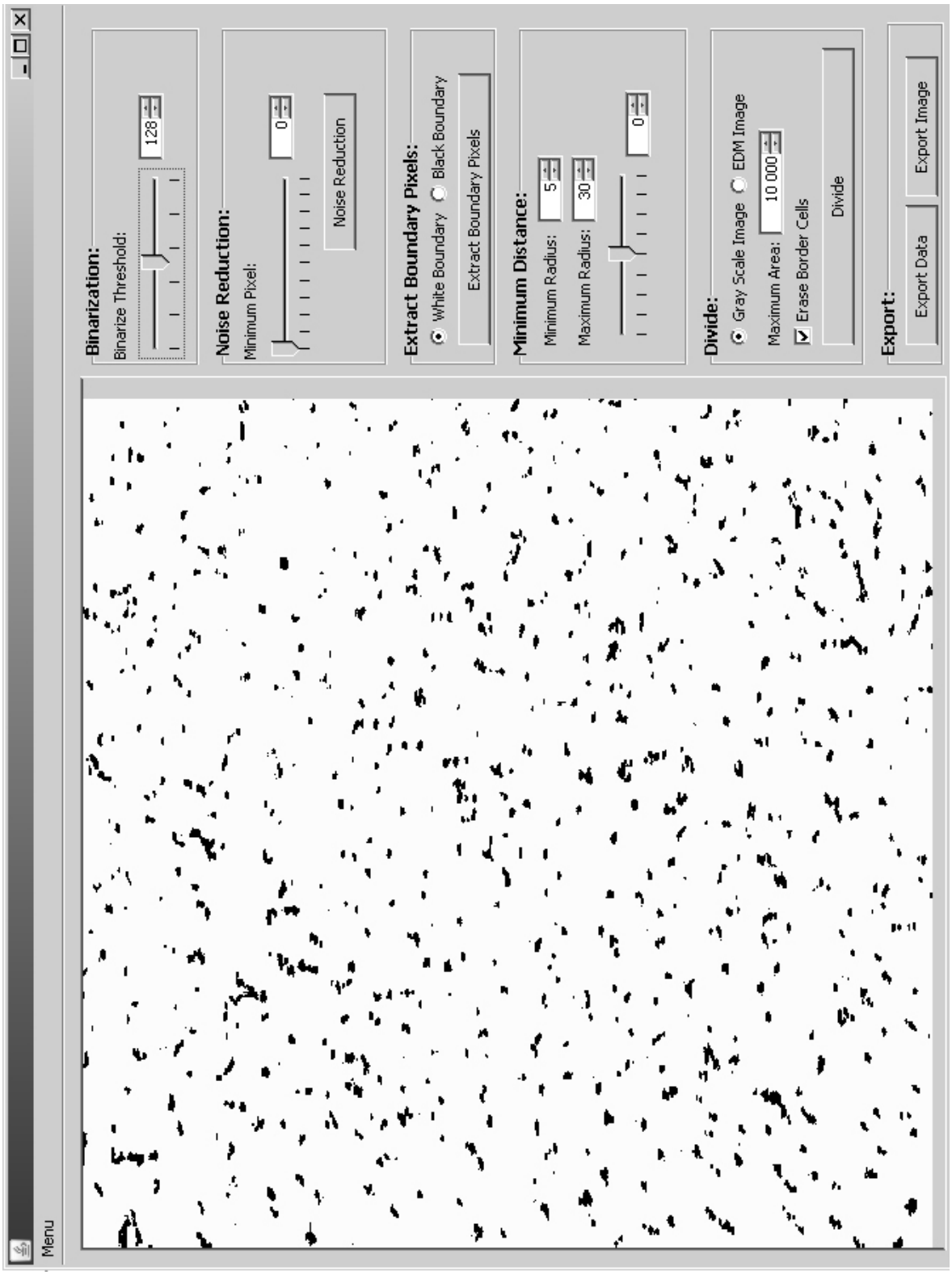

APPENDIX A II: SW TESSELLATION – BASIC COMMANDS

Binarization

By moving scroll box determines threshold between black colour (value = 0) and white colour (value = 255)

Noise Reduction

Erases the aggregates of noise pixels according to selected value.

Extract Boundary Pixels

Calculates the boundary foreground pixels, according to selected parameter (white or black boundaries).

Minimum Distance

Set of the maximal and minimal radiuses. The scroll box determines overlapping of circles (increasing value denotes decreasing overlapping, respectively.

Divide

Computates the "net" of pores boundaries.

Export Data

Exports results to the "***.dat**" file.

Export Image

Exports results to the "***.png**", "***.jpg/jpeg**" or "***.bmp**" file.

APPENDIX A III: VBA CODE FOR MODEL OF STRUCTURE

```
Cells(vybrany, sloupec).Interior.ColorIndex = 3
Next sloupec
End Sub
Sub vypocet1()
    Dim prum, sigm, pom As Double
    Dim radek, sloupec As Integer
    radek = 1
    For sloupec = 3 To 3 Step 1
       Sheets("List1").Select
       Cells(3, 13).Value = sloupec
          For prum = 20.5 To 20.5 Step 0.1
          For sigm = 4.6 To 4.6 Step 0.1
            pom = Rnd(-1)
            Randomize (prum * sigm * sloupec + 1)
            Sheets("List1").Select
            Cells(1, 13).Value = prum
            Cells(2, 13).Value = sigm
            pom = Cells(1, 16).Value
            Sheets("List2").Select
            Cells(radek, 1).Value = prum
            Cells(radek, 2).Value = sigm
            Cells(radek, sloupec + 2).Value = pom
            radek = radek + 1
          Next sigm
       Next prum
       radek = 1
    Next sloupec
    Sheets("List2").Select
    Range("C18").Select
End Sub
```